HiSST: 3rd International Conference on
High-Speed Vehicle Science & Technology
14-19 April 2024, Busan, Korea

Expansion Tube Capabilities for Studying Boost-Glide Re-entry Conditions

Yuhui Lin[1], *James J. Wallington*[2], *Thien Bui*[2], *Toby van den Herik*[2], *Christopher M. James*[3], *Eric Won Keun Chang*[4], *Tobias A. Hermann*[5]

Abstract

The expansion tube is a unique hypersonic impulse facility capable of producing both high-enthalpy and high total pressure conditions simultaneously through the unsteady expansion of a non-stagnated test flow. When coupled with high-performance free-piston or detonation drivers, expansion tubes allow for the simulation of such conditions as scaled Earth re-entry, scaled entry into the atmospheres of other planets in the solar system, and high-speed flight through the Earth's atmosphere. This paper focuses on the latter case and considers the capabilities of expansion tubes for re-creating the conditions experienced at various parts of the re-entry trajectory of a boost-glide vehicle. Boost-glide vehicles are a type of hypersonic vehicle which is generally boosted just outside the atmosphere by a rocket before 'gliding' down through the Earth's atmosphere to a target, often re-entering at very high-speeds for atmospheric flight of up to Mach 22 (greater than 6 km/s). In a military sense, they are strategically important and are currently being developed by several nations around the world. The expansion tube's unique ability to simulate high-enthalpy and high total pressure flight makes it particularly well suited to the study of these conditions. This paper will present expansion tube performance envelopes compared to planned boost-glide trajectories, as well as considering specific facility considerations required to generate these conditions.

Keywords: *expansion tube, shock tunnel, impulse facility, high-enthalpy testing, boost-glide, hypersonic glider, hypersonic waverider*

1. Introduction

The concept of a boost-glide hypersonic vehicle was first proposed by Sanger and Bredt in the 1930s and 1940s [1, 2]. Since then they have been considered on and off for many hypersonic flow scenarios, in both the civilian and the defence domains, for example [3–11]. A boost-glide vehicle operates exactly as its name implies. It is boosted to a high altitude and high speed, generally by a rocket, and then it glides, unpowered, to its destination [12–14]. A boost-glide vehicle by definition then, is a hypersonic glider or 'waverider' which under those names have also waxed and waned in popularity over the years, with many example studies and designs in the literature from the 1950s until today [15–25].

In recent years boost-glide vehicles have received much interest in the defence domain due to their ability to be launched similar to traditional intercontinental ballistic missiles (ICBMs), in many cases using similar launch hardware, but then being able to fly a lower, more manoeuvrable, and less easily detectable

[1]*Centre for Hypersonics, School of Mechanical and Mining Engineering, The University of Queensland, St Lucia, QLD, 4072, Australia, E-mail:yuhui.lin@uq.net.au*
[2]*Centre for Hypersonics, School of Mechanical and Mining Engineering, The University of Queensland, St Lucia, QLD, 4072, Australia*
[3]*Centre for Hypersonics, School of Mechanical and Mining Engineering, The University of Queensland, St Lucia, QLD, 4072, Australia, E-mail:c.james4@uq.edu.au*
[4]*Oxford Thermofluids Institute, Department of Engineering Science, University of Oxford, Osney Mead, Oxford OX2 0ES, United Kingdom, E-mail:ericwk.chang@eng.ox.ac.uk*
[5]*Oxford Thermofluids Institute, Department of Engineering Science, University of Oxford, Osney Mead, Oxford OX2 0ES, United Kingdom, E-mail:tobias.hermann@eng.ox.ac.uk*

trajectory to their target [12]. Seemingly related to this new interest in boost-glide vehicles, there seems to be an increasing interest in boost-glide vehicles and vehicles just defined as 'hypersonic glide vehicles' in the literature too, with many new papers in the last couple of years, such as [26–37].

Boost-glide systems are in development in the US and have been flight-tested in programs such as the Hypersonic Technology Vehicle-2 (HTV-2) program [38]. It is believed that Russia [39, 40] and China [41, 42] may have active boost-glide systems, though this is not necessarily independently verified.

Boost-glide trajectories involve re-entry speeds of up to Mach 22, which is greater than $6\,\mathrm{km/s}$. This means that these vehicles experience highly hypersonic flight and may remain as such for a large part of their trajectory. As an example, the severity of boost-glide conditions are in fact similar to later portions of a ballistic re-entry trajectory. Taking the Japanese Hayabusa asteriod sample return mission as an example [43], Hayabusa was predicted to be travelling at $6.9\,\mathrm{km/s}$ when it reached an altitude of $45\,\mathrm{km}$. This is similar to the speed and altitude of the US HTV-2 boost-glide vehicle when it begins to glide, as shown in Fig. 1 below. Boost-glide vehicles will spend extended periods of time at these conditions, making the study of heating during their trajectory very important.

Testing hypersonic flight at flight total enthalpy is generally performed in reflected shock tunnels (RSTs) or expansion tubes due to their ability to simulate hypersonic flight at both high enthalpy and relatively high total pressure. However, RSTs generally cannot simulate flows much faster than Mach 12 because they have to stagnate the gas at full total temperature and total pressure in the stagnation region which feeds the nozzle. These conditions become extreme fairly quickly as the Mach number increases and reflected shock tunnels are generally structurally limited to 150 to $300\,\mathrm{MPa}$ total pressure [44], and nozzle throat erosion becomes an issue at these conditions [45]. There is also the issue of test flow chemical freezing in their nozzles caused by the rapid expansion of test gas from the stagnation region through the nozzle to generate the test flow [46, 47]. For higher enthalpy and higher Mach number cases these effects will be more pronounced because the flow will both be heated to a higher temperature in the facility to generate the required total temperature, resulting in more flow dissociation, and even potential ionisation, and then expanded further to reach a higher Mach number.

This is where the expansion tube comes in. Similar to an RST, an expansion tube increases the test flow enthalpy by processing it with a moving shock wave, however, then instead of reflecting the shock off the end wall to generate more enthalpy, the flow is unsteadily expanded in a constant area tube, where extra enthalpy is added while the flow is actually cooling down. The maximum temperature of the test flow being decreased (for a given flow enthalpy) and the flow never being stagnated at full total pressure, means that there are no physical limitations on total pressure in an expansion tube. This makes the expansion tube especially suited to simulating high enthalpy and high total pressure flight such as planetary entry or very high Mach number atmospheric flight. When an expansion tube is combined with a powerful free-piston shock tunnel driver [48], such as UQ's X2 and X3 expansion tubes [49], Oxford's T6 facility [50] and JAXA's HEK-X facility [51], very high enthalpy test flows can be generated, which is why these machines are often used for simulating planetary entry. Furthermore, the higher total pressure capacity of the free-piston driver generally enables the simulation of subscale models with appropriate binary scaling [52–54] of the flow conditions.

An underutilised opportunity for expansion tubes is the simulation of high enthalpy, high total pressure, and high Mach number flight such as the Mach 20+ conditions experienced by boost-glide vehicles. Due to their ability to generate test conditions of both high enthalpy and high total pressure simultaneously, expansion tubes are uniquely placed to study boost-glide conditions, allowing the heat flux, flow radiation, and forces on these vehicles to be studied in a ground test environment. A caret waverider was tested in UQ's X3 expansion tube in the mid 2000s at $9\,\mathrm{km/s}$ equivalent flight speed in Silvester et al. [55], however, the results were mainly preliminary and there is much more work to be done. Likewise, the European Space Agency (ESA) Intermediate eXperimental Vehicle (IXV) wingless lifting re-entry vehicle [56], now called the Space Rider, has been tested in UQ's X2 expansion tube in several preliminary experimental campaigns [57–59], but there is much more to be done. The majority of experimental studies of hypersonic gliders and waveriders are at much lower enthalpy than they would fly

at in flight or for testing designs of low Mach numbers gliders, such as [34, 60–69] which allows a lot of phenomena to be studied, such as assessing high Mach number and high Reynolds number stability, lift over drag coefficients, surface pressure, convective flux, and shock shapes in Gillum et al. [60–62] and Norris et al. [64], but not the effect of the flow enthalpy on vehicle performance, and that is what we expansion tubes are well placed to study.

The goal of this paper is to examine how expansion tubes can be used to simulate boost-glide flight by comparing boost-glide trajectories to conditions which can be simulated in UQ's free-piston driven X2 expansion tube [49], which is one of the highest performance impulse wind tunnels in the world, in terms of the density-length ($\rho \cdot L$) product which it can generate at high enthalpy conditions. It is hoped that this work will lead to future boost-glide vehicle related experiments being performed in expansion tube facilities around the world. Future work aims to also examine the place for other expansion tubes around the world, such as cold and detonation driven facilities, and UQ's larger X3 expansion tube [49], but due to scope and time limitations, this paper will just focus on the X2 facility.

2. Boost-glide Trajectories

To understand how expansion tubes can simulate boost-glide conditions, we first need to know what boost-glide conditions look like. Due to their defence applications there is generally very limited info about real flight trajectories, but often modelling results can be found. Acton [12] modelled the trajectory of the US HTV-2 boost-glide vehicle [38] by using the limited available information about its two flight tests to simulate its two trajectories. The results are presented in Figure 4 of the paper. Here we have interpolated the raw data from those plots to produce the figures shown in Fig. 1. The top two figures show the altitude and velocity with distance, which were taken directly from Acton [12], and then we have done further processing to add the freestream density (from the U.S. Standard Atmosphere, 1976 [70]), stagnation enthalpy, Mach number, a heat flux type parameter by plotting $\sqrt{\rho} \cdot U^3$ which the convective heat flux scales with [71], the dynamic pressure ($\frac{1}{2}\rho U^2$), and the equilibrium total pressure and total temperature using equilibrium gas calculations done with UQ's Gas Dynamics Toolkit (GDTk) [72] backed by NASA's Chemical Equilibrium with Applications (CEA) program [73, 74].

Examining Fig. 1 it can be seen that the vehicle re-entered at speeds between 6000 and $7000\,\mathrm{m/s}$ and it cruised for a distance of around 6000 to $7000\,\mathrm{km}$. In both cases the altitude drops sharply from 100 to around $50\,\mathrm{km}$ over a distance of around $1000\,\mathrm{km}$ where the trajectories then begin their extended glide over a distance of more than $5000\,\mathrm{km}$. From our basic analysis it can be seen that the glide begins around Mach 20 for the faster B flight and that peak heat flux occurs shortly after the glide begins for both flights. Dynamic pressure is around $20\,\mathrm{kPa}$ at the start of the glide, and increases to around $50\,\mathrm{kPa}$ for the B flight and $40\,\mathrm{kPa}$ for the A flight at the end of the glide. Both vehicles are still hypersonic at the end of the glide, with the A flight ending the glide with a Mach number of 7.26 and the B flight ending the glide with a Mach number of 8.16.

It is also interesting to note the scale of the equilibrium total pressure and temperature for both trajectories. For the slower A flight the equilibrium total temperature peaks at around $9000\,\mathrm{K}$ at the start of the trajectory before the glide begins. For the faster B flight it peaks around $10\,000\,\mathrm{K}$ just before the glide begins. For both trajectories, the total pressure climbs as the altitude drops before starting to drop throughout the glide phase as the atmosphere slows the vehicle down. For the slower A flight the total pressure peaks at around $2\,\mathrm{GPa}$ and for the faster B flight it peaks at around $4.5\,\mathrm{GPa}$. These are very high total temperatures and total pressures, and as noted in the introduction, the total pressures far exceed the structural limitations of reflected shock tunnels of up to $300\,\mathrm{MPa}$ [44] showing that other types of facilities such as expansion tubes are needed to simulate these conditions.

As peak heating is generally an important trajectory point for design and for expansion tube testing, the peak heating point for each flight is shown as vertical lines in Fig. 1 and we have tabulated important values at these conditions in Table 1 below. Freestream density, temperature and pressure were found using the US Standard Atmosphere, 1976 [70] at the flight altitude.

Examining the table it can be seen that for the A flight peak heating occurs at an altitude of $47.38\,\mathrm{km}$, with a freestream velocity of $5472\,\mathrm{m/s}$ at a Mach number of 16.59, a stagnation enthalpy of $14.97\,\mathrm{MJ/kg}$,

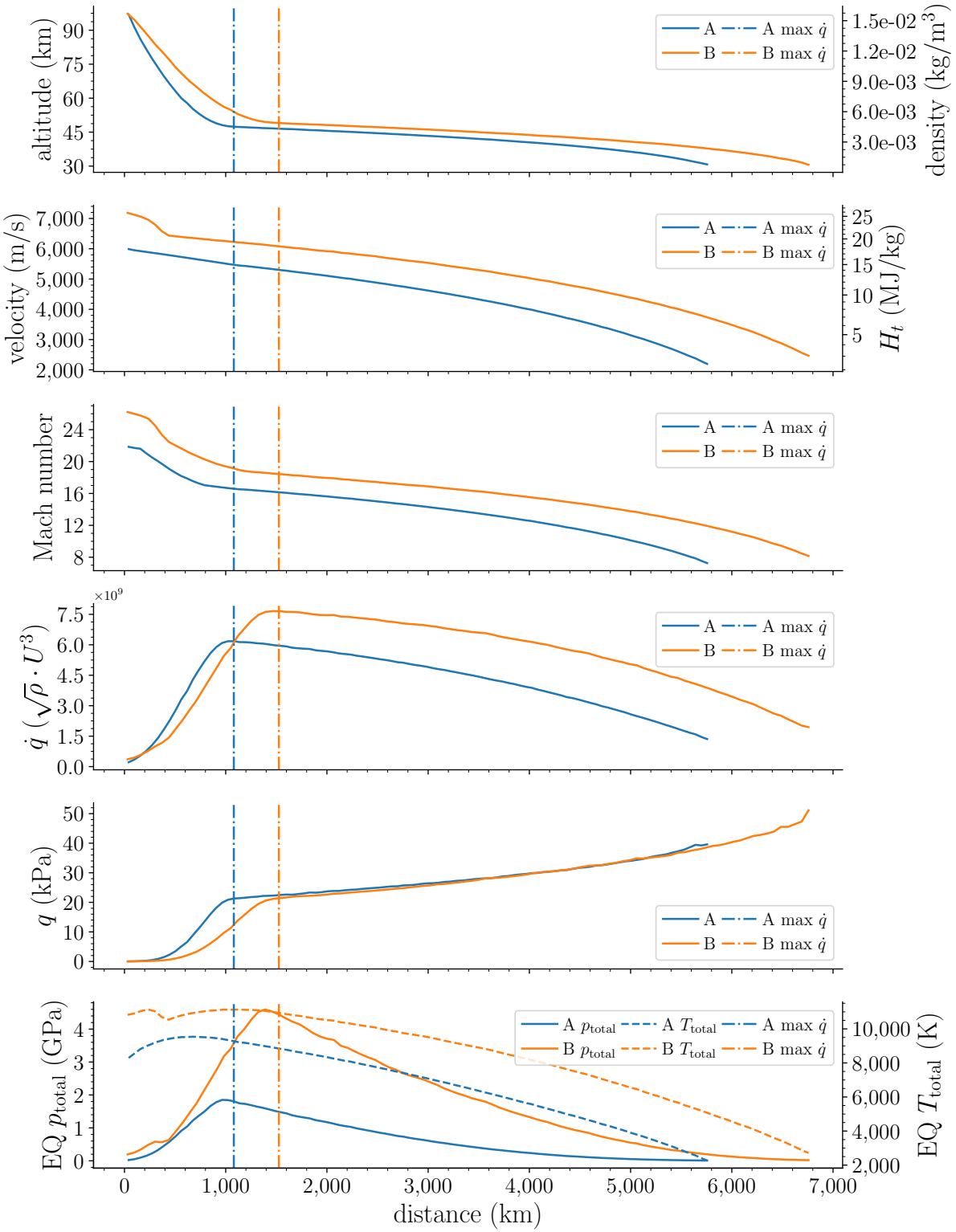

Fig 1. Simulation of the US HTV-2 boost-glide vehicle trajectory from Acton [12] with further analysis showing the related density, stagnation enthalpy, Mach number, scaled heat flux, and dynamic pressure.

Table 1. Peak heating data for the simulation results shown in Fig. 1 from Acton [12].

Variable	A flight	B flight
Distance (x, km)	1,080	1,526
Altitude (h, km)	47.38	49.01
Freestream Velocity (v_∞, m/s)	5,471	6,080
Mach Number (M_∞)	16.59	18.43
Freestream Density (ρ_∞, kg/m^3)	1.42e-03	1.16e-03
Freestream Temperature (T_∞, K)	270.65	270.65
Freestream Pressure (p_∞, Pa)	110.52	90.18
Dynamic Pressure (q, kPa)	21.29	21.45
Pitot Pressure (p_{Pitot}, kPa)	42.59	42.90
Stagnation Enthalpy (H_t, MJ/kg)	14.97	18.48
Equilibrium total pressure (p_{Total}, GPa)	1.81	4.45
Equilibrium total temperature (T_{Total}, K)	9277.92	10937.87

and an equilibrium total pressure of 1.81 GPa. The slightly faster B flight has a peak heating altitude of 49.01 km, occurring at a freestream velocity of 6080 m/s at a Mach number of 18.43, a stagnation enthalpy of 18.48 MJ/kg, and an equilibrium total pressure of 4.45 GPa.

The peak heating point of the slightly faster B flight shown in Table 1 is the trajectory point which we will try to match on the X2 facility in Section 4 as the higher enthalpy and total pressure is more of a stress test on what can be simulated in a free-piston driven expansion tubes.

3. Scaling a Boost-Glide Vehicle for Testing in an Expansion Tube

There are many boost-glide vehicle designs which could be considered for testing in an expansion tube. The US HTV-2 vehicle geometry was chosen due to it being a flight-tested geometry, its high enthalpy somewhat well known trajectory, and it being a popular geometry for simulations (such as in a lot of the recent papers discussed in the introduction). It also happens that we recently completed a project in our laboratory where we tested a HTV-2 model in a small teaching reflected shock tunnel to perfect techniques for testing free-flying gliders in X2 in the future in Bui [75], so we had a version of the geometry which we could easily use. While generally specific information about boost-glide vehicles is limited, Bui [75] made a HTV-2 CAD model geometry from information about the geometry found in Zhang et al. [76] which appeared to at least approximately match other information which could be found publicly about the vehicle. As only the leading dimensions are important here, as opposed to how well any fine details are modelled, the solid model from Bui [75] was used to size a potential model to be tested in our X2 expansion tube facility in this work.

As the HTV-2 is long and fairly thin the main parameters which are important for sizing a HTV-2 test model for a test facility are the vehicle's length, which will be scaled to suit the facility, and its angle of attack (AoA), which controls whether the model will be a long thin object in the core flow, or an object facing up or down in the core flow at potentially a large angle. In Zhang et al. [76], the length of the HTV-2 vehicle was stated to be 4 m which seemed suspiciously clean for a leading dimension on a US vehicle, so we looked further and found that in Niu et al. [77], another contemporary Chinese paper with analysis of hypersonic glide vehicles, the HTV-2 length is shown in Fig. 9 of that work to be 3.67 m long, which being 12 feet seems more realistic for a US vehicle. A modern US paper, Tracy and Wright [14], also uses the 3.67 m, which is attributed to Niu et al. [77]. A very recent Italian paper, Ragnoli et al. [26], references their geometry to Tracy and Wright [14]. This length is corroborated by media reports we could find about the HTV-2 vehicle from around the time it flew, such as [78] which states that the vehicle is 12 foot long. So the model length for scaling the vehicle was set at this 3.67 m value.

Finding AoA was harder, with little information available about the actual HTV-2 vehicle and its flights in this regard. For example, while the work of Acton [12], whose trajectory data from flight simulations of the HTV-2 test flights was used in Section 2, was probably calculating AoA in real time throughout the trajectory, these values are not shown in the paper. Bui [75] looked in the literature and found papers such as [11] which stated that the L/D ratio, which needs to be maximised to maximise the length of the glide, for a hypersonic glide vehicle appears to peak for AoA values from 5 to $15°$. This was approximately corroborated by other similar studies, such as Niu et al. [77] that stated that the AoA range of a HTV-2 like hypersonic glider would be 0 to $30°$ and Li et al. [10] where the maximum AoA is $20°$. The recent Italian aerothermal analysis paper [26] used an AoA of $15°$ for their CFD simulations. Due to this large variation in AoA values, which probably reflects both uncertainty in actual knowledge of these flights and also the fact that the AoA would change during a flight, example calculations of achievable model size have been performed for an AoA range from 5 to $30°$.

Now that we know the size of the model at full-scale and its approximate AoA range, we can consider the scaling factor required for experiments on a particular facility. We will use our X2 expansion tube at UQ as an example, but a similar analysis could easily be performed for other facilities as well. X2 has a nozzle exit diameter of 201.8 mm and when the flow exits the nozzle a Mach wave forms between the core flow exiting the nozzle and the quiescent gas in the test section, which moves inwards at the Mach angle, creating the outer half of the core flow diamond. This means that the core flow is also a function of the flow Mach number, so we will need to consider conditions at different Mach numbers. We performed calculations at Mach numbers of 10, which is X2's nozzle exit design Mach number [79], 12, 16 and 18 to consider higher Mach number conditions seen in a boost-glide trajectory up to the HTV-2 predicted peak heating Mach number of around 18 from our analysis of the Acton [12] HTV-2 simulations in Section 2.

While the core flow diamond is mirrored inside the facility's nozzle, and the technique of placing the test model in as much of the core flow diamond as possible is used by a lot of hypersonic test facilities to maximise model size within blockage limits, we have chosen to use only the external, test section part of the core flow here due to the limited test times generally available in expansion tubes anyway. If an expansion tube facility had particularly long test times, this analysis could be redone with the model placed in the nozzle too to further increase the maximum model size. Placing the model half inside the nozzle also prevents optical access to the front of the model, which we would prefer to avoid.

An analysis in Python was used to work out which scaled size HTV-2 test models could be tested in X2 for different X2 nozzle exit Mach numbers and different AoA values. The analysis uses the geometry of the model, the facility's nozzle exit diameter, and the Mach cone for the given test flow Mach number to ascertain how big of a model could be placed in the core flow for that condition. The results were then manually checked in CAD to ensure they were sensible and correct. The results of this analysis can be seen in Table 2 for AoA values from 5 to $30°$ and nozzle exit / test flow Mach numbers from 10 to 18. An example result showing a model in the X2 core flow can be seen in Fig. 2 below.

Table 2. Maximum model scale possible for testing a scaled HTV-2 glider model in UQ's X2 expansion tube for different model AoA and nozzle exit Mach numbers.

	Nozzle Exit Mach number			
Model AoA (degree)	10	12	16	18
5	12.6	11.9	11.2	10.9
10	12.5	11.9	11.1	10.9
15	12.4	11.9	11.1	10.9
20	12.4	11.8	11.2	10.9
30	13.4	13.0	12.6	12.4

Considering the results in Table 2, it can be seen that smaller scaling factors are generally required at smaller AoA as the model is more flat in the flow, with a small reduction at the minimum AoA ($5°$)

as eventually the model being too flat pushes it outside the core flow at the back of the model where the model is widest and the core flow is smallest. It can also be seen that the higher the test flow Mach number, the smaller the scaling factor required as the Mach angle becomes flatter at higher Mach numbers, this is taken to extremes for the Mach 18 freestream, where the minimum scaling factor is the same for every AoA except the final 30° case. Scaling factors of around 10 are reasonable, as X2 generally has the spare performance available to simulate flows at the increased density that is generally required to do this, which shows the potential for future experimentation.

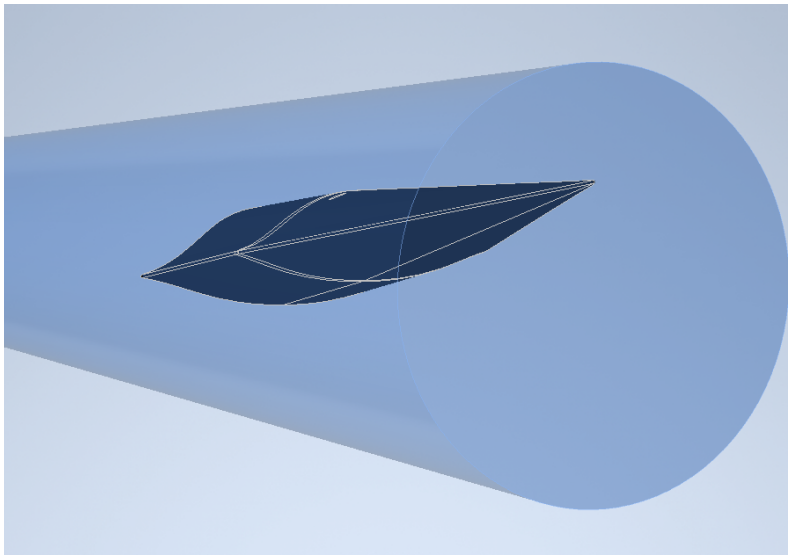

Fig 2. Schematic showing an example HTV-2 model in the X2 expansion tube core flow.

Another consideration is the potential need to image the whole test model optically for model tracking in free-flying model force measurements or other optical experimentation which may be required. If this is required, the model size is further restricted using X2's standard 192 mm diameter windows with a usable diameter of 180 mm. An example of this is shown in Fig. 3 below. This constrains the model scale to 20, half as big as if this consideration is not needed. However, due to the short test times in expansion tubes, this is probably the more realistic scaling factor for X2, so this scaling factor will mainly be considered for further work in this paper, with checks on the available flow lengths to be done in later sections of this work.

4. X2 Expansion Tube Capabilities for Studying Boost-Glide Vehicle Re-entry Conditions

This section will use the equilibrium gas expansion tube simulation code PITOT3 [80, 81] to generate theoretical performance maps showing how UQ's X2 expansion tube [49] could be used for the simulation of boost-glide vehicles targeting the peak heating point of the HTV-2 B flight which is shown in Table 1. A model scaling factor of 20 was chosen based on analysis in Section 3, which means the conditions to be simulated must achieve a freestream density scaled up by this factor to maintain the density-length or '$\rho \cdot L$' product, so the chemical length scales and the flow Reynolds number remain consistent with the actual flight (this is discussed further in Section 5.2). Specific considerations which need to be understood and managed for the simulation of high-enthalpy and high-total pressure conditions such as these will then be discussed in Section 5, similar to how expansion tube generation of high-speed Earth re-entry conditions were considered in James et al [82].

To assess the feasibility of using expansion tubes to study the flight of boost-glide vehicles, PITOT3 was first used to perform simulations for a range of shock tube fill pressures from 20 to 500 kPa, and a range of acceleration tube fill pressures from 20 to 1000 Pa. 30 logarithmically-spaced pressure values were used for both of these fill conditions respectively, across multiple X2 expansion tube free-piston driver

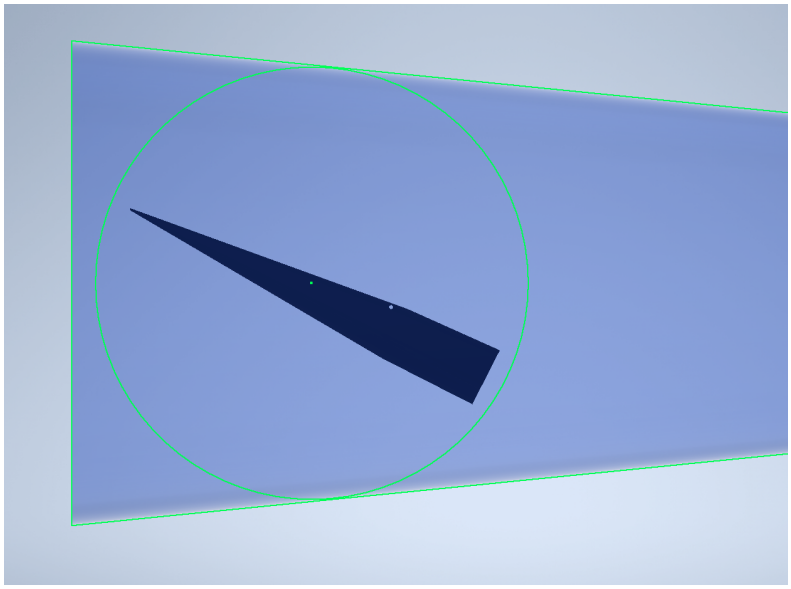

Fig 3. Schematic showing an example HTV-2 model in the X2 expansion tube core flow which is constrained by the available maximum window size.

conditions. The results of each simulation are presented as individual scatter plots of flight equivalent velocity, essentially the flow velocity if any flow stagnation enthalpy from chemical means caused by a potentially elevated facility freestream temperature was turned into velocity (i.e. $H_t = \frac{1}{2}U_e^2$), against freestream density in Fig. 4 below. The interpolated HTV-2 trajectory results from Acton [12] presented in Section 2 are also shown on the plot at flight scale and with densities 10 and 20 times the flight value to simulate $\rho \cdot L$ scaling factors of 10 and 20.

In general, in Fig. 4 it can be observed that the X2 expansion tube is capable of producing test conditions with appropriate flight equivalent velocity and density, that covers a large portion of the trajectory of the HTV-2 vehicle at the scaling factors required. It should be noted that the high density and low velocity region of the flight, where the altitude is much lower, may be outside the current the operation envelope of X2, or at least outside the regions which were simulated to produce Fig. 4. If these trajectories were ever of interest for testing in X2, further investigation into these trajectories could be done, as they might require higher fill pressures or new lower compression ratio drivers or higher molecular weight drivers, as X2's lowest performance current free-piston driven condition has a compression ratio of 20 and uses 80%He/20%Ar (by volume) which still leads to driving quite a strong shock. While the free piston driver is generally used for its high performance, in recent years there has been success with designing new 'low performance' free piston driver conditions to extend the operating envelope of these facilities at the lower end, such as in Chan et al. [83] and Stennett et al. [84].

As mentioned in Section 2, the peak heating point of HTV-2 B flight is the point of interest for this study. This point with its density scaled by 20, as indicated by the intersection of the lines in the middle of Fig. 4 at $(U_e = 6080\ m/s,\ \rho = 0.0232\ kg/m^3)$, can be observed to lie comfortably in the operation region of multiple driver conditions. The fill conditions of the simulations represented by the scatter points close to the intersection were identified, and refined simulations were performed with conditions in the proximity of these regions. The results for the 4 most powerful driver conditions of X2 are presented in Fig. 5 below, with the results now plotted on contour plots with the facility freestream Mach number (M_8) on the z-axis.

From the performance maps in Fig. 5, it can be observed that while different X2 driver conditions can achieve the required flight equivalent velocity and freestream density, none of the conditions reach the required freestream Mach number of 18, with the freestream Mach number at the design point

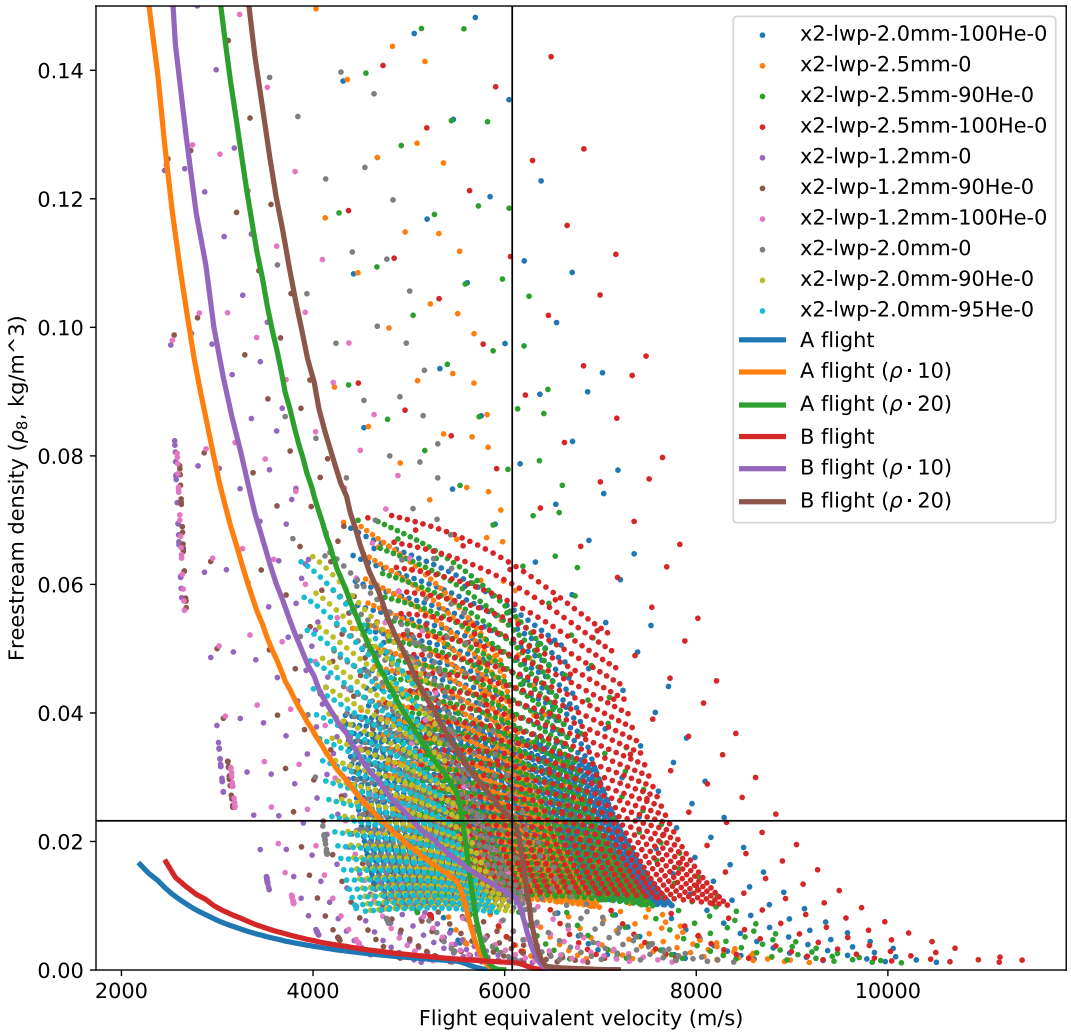

Fig 4. Simulated flight equivalent velocity vs freestream density for the X2 expansion tube using many different facility driver conditions.

instead ranging from arund 12.5 to around 16, depending on the individual driver condition. This is occurring because more powerful driver conditions with 90%He/10%Ar (by volume) or 100%He driver compositions are able to generate the required flight equivalent velocity and freestream density with a higher shock tube fill pressure (p_1) and a lower acceleration tube fill pressure (p_5), this means that the shock tube shock speed (v_{s1}) is lower for a similar acceleration tube shock speed (v_{s2}) meaning the flow is shocked less and unsteadily expanded more, resulting in a higher Mach number. The potential ramification of not being able to re-create correct at the correct Mach number is discussed in detail in Section 5.6.

Through the refined simulations, the test conditions shown in Table 3 were identified to be the best representations of the HTV-2 B flight peak heating point. These test conditions were able to produce both flight equivalent velocity and test flow density values within 0.11% of the target values of 6080 m/s and 0.0232 kg/m^3. Multiple conditions have been chosen as different driver conditions may end up being more optimal in reality when tested on the facility. Based on these results, it appears that the X2 expansion tube is a suitable facility to test boost-glide vehicles. However, there are a range of potential issues to be worked through in terms of practically simulating these conditions, which are discussed in

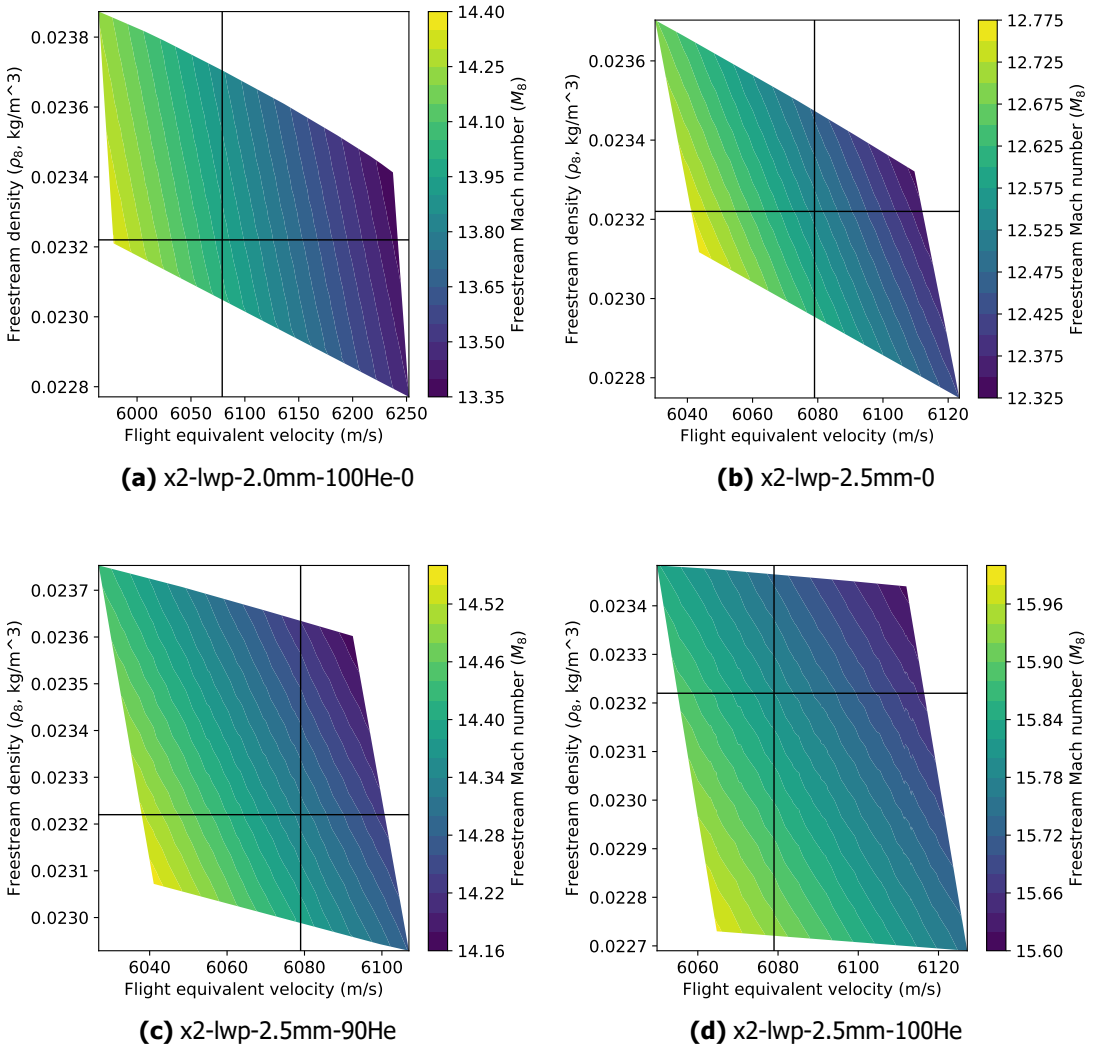

(a) x2-lwp-2.0mm-100He-0

(b) x2-lwp-2.5mm-0

(c) x2-lwp-2.5mm-90He

(d) x2-lwp-2.5mm-100He

Fig 5. Performance maps of X2 expansion tube for simulation of US HTV-2 boost-glide vehicle peak heating point

Section 5.

5. Unique Characteristics of These Test Conditions

The majority of expansion tubes around the world are used for generating conditions related to planetary entry, generally at equivalent flight speeds of $6\,\mathrm{km/s}$ and above but at the fairly low densities associated with the peak heating point of re-entry trajectories which generally occur at high altitudes where the freestream density is low. This is especially true for conditions generated in cold driven expansion tube facilities where test conditions available are limited by the facility driver. Even in high-performance free-piston driven expansion tube facilities, often the high-performance is used to generate higher enthalpies instead of higher densities.

While generating mid enthalpy, high density conditions in expansion tubes is not unheard of, due to it being less common, some of the unique issues related to generating these types of conditions will be discussed below, with further analysis or discussion of results from Section 4 discussed here where it is needed.

Table 3. X2 expansion tube parameters for simulating peak heating point of HTV-2 flight B

Candidate	1	2	3	4	5	6
Driver Condition	x2-lwp-2.0mm-100He-0	x2-lwp-2.5mm-0	x2-lwp-2.5mm-90He-0		x2-lwp-2.5mm-100He-0	
Shock Tube Fill Pressure (p_1, kPa)	137.59	94.44	150.33	151.44	210.56	211.67
Acceleration Tube Fill Pressure (p_5, Pa)	257.22	286.56	251.33	251.33	231.67	231.67
Flight Equivalent Velocity (U_e, m/s)	6081.23	6079.47	6079.61	6072.41	6081.92	6075.10
Freestream Density (ρ_8, m/s)	0.02321	0.02324	0.02321	0.02322	0.02322	0.02322
M_7	10.18	9.24	10.42	10.43	11.36	11.37
Mach Number (M_8)	13.97	12.53	14.33	14.36	15.79	15.82
a2 (a_2, m/s)	1058.7	1078.1	1054.0	1052.9	1037.7	1036.7
a3 (a_3, m/s)	2619.7	1437.3	1884.2	1885.7	2748.0	2749.2
a_2/a_3	0.4041	0.7501	0.5594	0.5584	0.3776	0.3771
v_{s1}	2748.83	2835.12	2728.90	2724.33	2661.21	2657.32
v_{s2}	5977.06	5938.77	5982.99	5976.62	6010.29	6004.01
v_{s1}/v_{s2}	0.4599	0.4774	0.4561	0.4558	0.4428	0.4426
Test Time (t, μs)	94.16	105.62	91.72	91.66	83.02	83.00
Slug Length (m)	0.5699	0.6370	0.5553	0.5544	0.5040	0.5033
Pitot Pressure (kPa)	818.91	814.80	819.35	817.98	823.49	821.64
Total Pressure (GPa)	19.66	11.57	22.22	22.30	35.39	35.44
Stagnation Enthalpy (Ht, MJ/kg)	18.49	18.48	18.48	18.44	18.49	18.45
T_7	890.17	1079.82	849.82	844.90	714.08	710.55
T_8	469.25	584.10	445.45	442.56	367.49	365.50

5.1. High Enthalpy and High Pressure

The first requirement of simulating boost-glide conditions is the need to generate conditions at relatively high enthalpy, up to around $6\,\mathrm{km/s}$ flight equivalent velocity considering the results presented in Section 2 above for the HTV-2 vehicle, but also relatively high density. The HTV-2 altitude at peak heating is around $48\,\mathrm{km}$ (see Table 1) where the freestream density is around $1.0 \times 10^{-3}\,\mathrm{kg/m^3}$. Comparatively, the Hayabusa superorbital Earth re-entry peak heating, point which occurred at $58\,\mathrm{km}$ altitude at a freestream density of $4.0 \times 10^{-4}\,\mathrm{kg/m^3}$ [43], is 2.5 times lower density.

An issue when comparing something like Hayabusa to the HTV-2 is the relative vehicle size. Hayabusa has a $0.4\,\mathrm{m}$ diameter but the HTV-2 is $3.67\,\mathrm{m}$ long, almost 10 times larger. This makes it a similar size to the Apollo capsule which had a diameter of $3.9\,\mathrm{m}$ and which required X2's highest performance driver conditions to generate scaled conditions to simulate Apollo peak heating [85]. Binary scaling, where flow total enthalpy or 'flight equivalent velocity' is conserved as well as the product of the flow density with a characteristic length scale (i.e. the ρL product) approximately scales binary chemical processes like dissociation and also Reynolds number [52–54], both of which are important for ensuring a tunnel experiment is comparable to flight when things like chemistry and convective heat transfer are important. The issue then becomes generating the conditions not at the required flight density, but at a density much higher than this. In Section 3 it was found that scaling factors for HTV-2 vehicles on X2 would be from 10 to 20 depending on the experimental requirements, with 20 seeming to be the most realistic scaling factor. This means that conditions much be generated at $6\,\mathrm{km/s}$ flight equivalent velocity at a freestream density of $1.0 \times 10^{-2}\,\mathrm{kg/m^3}$ which is quite demanding, and as can be seen in Section4, this requires some of X2's most powerful driver conditions, and X2 is very high performance tunnel. This means that without a free-piston driver the conditions are probably impossible to generate at that scale.

There are several other options to combat the issue of generating high enthalpy and high density conditions at binary scaling factors of 10 or 20. Firstly, bigger facilities than X2 with its driven tube diameter of $85\,\mathrm{mm}$ could be used, such as UQ's X3 free-piston driven expansion tube with a $200\,\mathrm{mm}$ driven tube diameter [86], HYPULSE which is now being recommissioned at Purdue University with a $6\,\mathrm{inch}$ ($152\,\mathrm{mm}$) driven tube diameter [87], or LENS-XX with a $2\,\mathrm{foot}$ ($600\,\mathrm{mm}$) driven tube diameter [88]. All of these facilities also have nozzles so like X2 they can benefit from testing model scales larger than the driven tube diameter. While all of these facilities have less powerful drivers than X2, their large scales reduce performance requirements so they might also be able to simulate the required conditions.

The other consideration is just simulating other parts of the trajectory which occur at lower enthalpy. While peak heating is important for obvious reasons and being close to maximum stagnation enthalpy drives chemistry, which is part of the reason for wanting to simulate these conditions in expansion tubes in the first place, there are surely interesting phenomena related to boost-glide vehicles which could be studied in cold driven expansion tubes at lower enthalpy or even phenomena to be studied which does not need to be scaled at all, removing the requirement to generate conditions at much higher freestream densities than flight.

One thing which we have done here as well is to scale the *freestream* density for binary scaling as in this work we are attempting to generate a freestream Mach number as close to flight as possible as we believe that this is important for re-creating the flow around a non-blunt re-entry vehicle. Generally expansion tubes use blunt body test models such as capsules, spheres and cylinders which are assumed to be 'Mach number independent'. (The reality of this for a boost-glide vehicle is discussed later on in Section 5.6.) Expansion tube test flows generally re-create flight total enthalpy, but at much lower Mach number, generally Mach around 7 if a nozzle isn't used and up to Mach 10 or 12 with a nozzle. This means that the bow shock over the model is weaker, and less total pressure is lost across the shock. If the *post-shock* state is scaled instead of the freestream state, less facility performance is required. Whether that is valid or not for a non-blunt geometry is up for debate, but it is an option if it is required.

5.2. The Effect of Large Scaling Factors

As was seen in Section 3, scaling factors of 10 to 20 will be required to simulate a HTV-2 vehicle in X2, which requires the test conditions to be generated at 10 or 20 times the flight density to re-create the post-shock chemical length scales and the Reynolds number of the flow through binary scaling [52–54]. While binary scaling is generally associated with blunt body flows, a review paper by Stalker [89] discusses a paper by Inger [90] which states that binary scaling is also applicable for slender bodies with a blunt nose, which may be considered similar to a HTV-2 vehicle. However, this similarity requires that the product of the freestream Mach number and a body thickness parameter τ (i.e. the $M_\infty \tau$ product) are also constant between the two flows, which either requires freestream Mach number to be re-created, or the geometry of the model to be changed, which may not be possible. Further discussions about the required Mach number can be found in Section 5.6.

An issue which may arise here when binary scaling the conditions is that technically binary scaling is not applicable for equilibrium flows because the equilibrium composition is in itself a weak function of pressure, and 10 or 20 are not necessary small scaling factors. This means that the post-shock state generated may not fully represent what would be seen in flight, and the increased post-shock density of the scaled case would be likely to suppress chemical reactions leading to less dissociation and a higher post-shock temperature. However, the equilibrium state is quite complex and in the enthalpy and density range considered here, it may not have a large effect either, so it is worth investigating.

To examine this approximately, calculations were done by performing a wedge shock with CEA [73, 74] at different AoA for the flight condition at flight scale, and with scaling factors of 10 and 20, to examining the effect of the scaling on the wedge shock angle and the ratios of flow properties across the shock. An AoA range from 0 to 30° was chosen to match the AoA values considered in Section 3, which are wedge angles from 3.43 to 33.43°, as the angle of the wedge on the bottom of the HTV-2 is 3.43° according to [76]. The results are presented in Fig. 6 below.

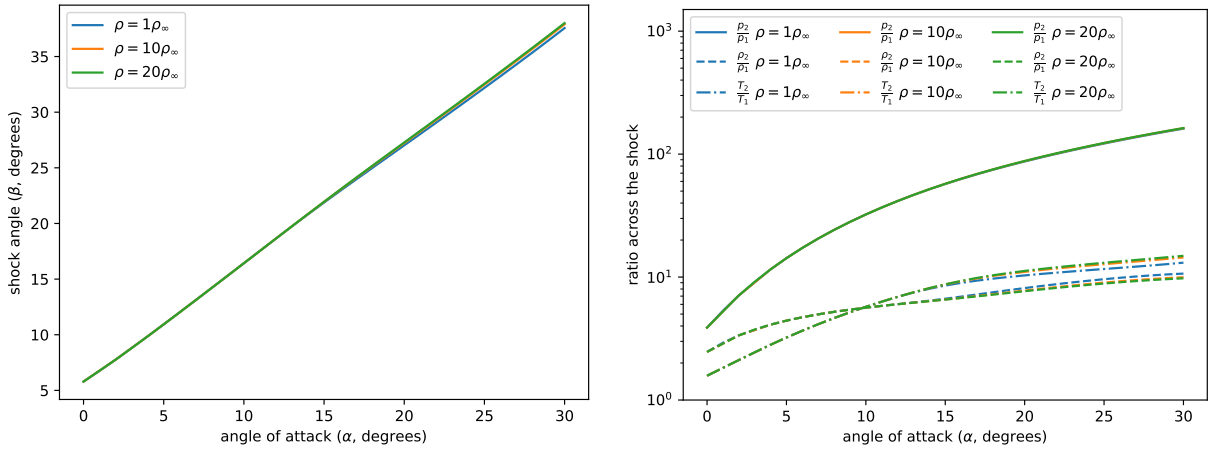

(a) effect on the oblique shock angle (β)

(b) effect on ratios across the shock

Fig 6. The effect of angle of attack and binary scaling factor on the oblique shock angle (β) and ratios across the shock.

In Fig.6a, where the effect of the scaling on the oblique shock angle (β) is shown, it can be seen that the scaling has a very small effect on β, which starts at an AoA of around 15°, but is still barely noticeable on the plot at the maximum angle of 30°. In Fig. 6b the effect of scaling on the ratios across across the shock are shown. Examining the figure it can be seen that the scaling does not appear to effect the pressure ratio across the wedge shock at all. Only small changes are seen in the temperature and density ratios across the shock, and even then they are confined to the highest AoA values where the strongest shocks will be occurring. In the main, this seems to show, at least approximately, that the

scaling factors required to test these conditions in X2 do not adversely affect the post-shock conditions generated. In saying that though, this basic analysis only considers the post-shock equilibrium flow over a wedge, which does not consider the fully 3D shape of a boost-glide vehicle or the effect that the scaling may have on the flow in the boundary layer flowing over the model, which is where convective heating, shear stress, and turbulence occurs.

5.3. Test Time Limitations - Can We Get the Required Flow Lengths at the Required Model Scale?

While there is a physical limitation to the scale of model which can be tested in a facility, as was discussed in Section 3, there is also a temporal limitation to start the flow over the model in the test time generated by the facility. As expansion tubes generally have test times an order of magnitude lower than similar sized reflected shock tunnels, test time is likely to be an important limitation for boost-glide vehicle testing in expansion tubes. X2 generally has a test time of around $100\,\mu$s for most conditions and from Table 3 it can be seen that the conditions proposed here are around that value with test times ranging from 83 to $106\,\mu$s depending on the exact condition.

The way to ascertain whether a model is likely to start is to consider the length of the test slug, which is the flow velocity multiplied by the test time, which gives a length when the flow can be considered steady, and then divide it by the model length to give the amount of "flow lengths" that the model experiences, which can then be compared to data about the establishment time of different processes, which are generally also expressed as an amount of flow lengths. The slug length of each condition is shown in Table 3 and they range from $0.5\,$m to $0.64\,$m.

The amount of flow lengths can be found with the following equation:

$$\text{flow lengths} = \frac{tU_\infty}{L} \tag{1}$$

where t is the facility test time and L is model length or sometimes D for model diameter it used. This is basically the same equation as Holden's equation for the characteristic flow establishment time, T, in a hypersonic wind tunnel experiment, which is the amount of flow lengths for the flow to fully start:

$$T = \frac{\tau_{est} U_\infty}{L} \tag{2}$$

where τ_{est} is the flow establishment time.

The issue then becomes one of how many flow lengths is required, but this is not so simple and is more of a guide than a hard science. Outside of doing one's own transient simulations of their particular proposed model at their proposed conditions, it is necessary to use what is available as a guide for one's own experiment.

Hornung [91] states that a 'reasonably conservative value' for flow establishment is 20 flow lengths, which is a good estimation but potentially too demanding for facilities like expansion tubes with particularly short test times. For windward flows, it is believed that only several flow lengths is required, which appears to originate from Davies and Bernstein [92] who state that 3.33 flow lengths is required to start the boundary layer over a flat plate. This number of around 3 flow lengths for windward flows is backed up by the popular CFD result from Lee and Lewis [93] for flat plates and similar papers such as Zhang et al. [94] who does similar simulations for scramjet internal flow paths and finds a similar result.

Leeward and separated flows are much harder to start, and it is generally believed that many 10s of flow lengths are required to start separated regions of flow, such as compression corners and wake flows, placing extreme limitations on experimental facilities in that regard. The common canonical result from Holden [95] states that 27.9 flow lengths are needed to start the pressure in a separated flow, and more than double that for heat transfer. Park et al. [96] experimentally examined flow establishment times for wake flows in a reflected shock tunnel and found that between 50 and 100 flow lengths were required

depending on the exact geometry and whether steady pressure or heat flux was being considered. Like in Holden [95], it took longer for the heat flux to stabilise. In a later paper, Park et al. [97] examined flow establishment times in the wake behind a small capsule in our X2 expansion tube and found that the pressure behind the model took about 15 to 20 flow lengths to stabilise and like their earlier work [96] and Holden's work [95] the heat flux took roughly twice as long.

In Fig. 7 an approximate test time of $100\,\mu s$ and a flight velocity of the HTV-2 B flight peak heating point of $6080\,m/s$ from Table 1 was used with the full length $3.67\,m$ HTV-2 scaled down 10 and 20 times to examine the amount of flow lengths available. As the AoA of the model changes, its horizontal dimension has been used to calculate the amount of flow lengths as that defines the physical space that the model takes up in the test slug length. For this reason, the flow length changes slightly with AoA as the length of the model in the x-dimension changes as it pitches up or down with AoA.

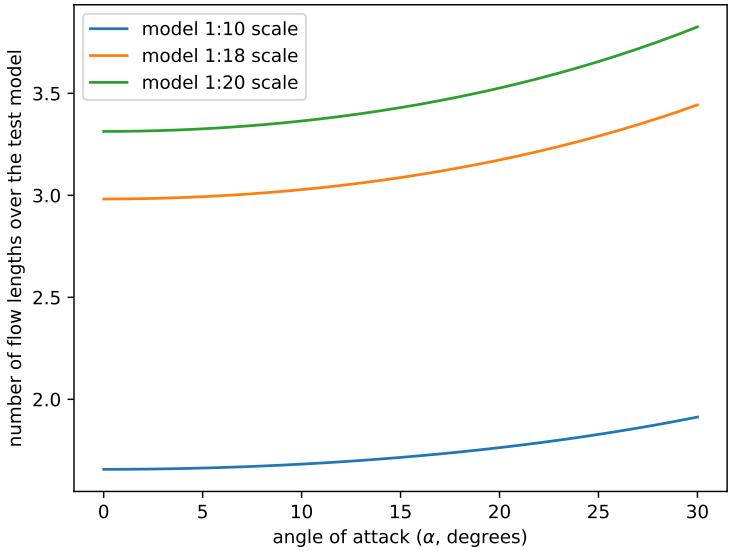

Fig 7. Angle of Attack versus flow lengths for different HTV-2 model scaling factors in X2.

In Fig. 7 it can be seen that with a scaling factor of 10, there are always less then 2 flow lengths over the test model, so this is clearly too large of a model to be tested in X2. With a scaling factor of 20, there are from 3.31 to 3.82 flow lengths over the model depending on the AoA selected, meaning that all of the potential AoA values have almost exactly or more flow lengths than the 3.33 flow length number for windward flows suggested by Davies and Bernstein [92]. A scaling factor of 18 was also added, which is the smallest scaling factor which was around 3 or above 3 for the whole AoA range. This results shows that around 1:20 scale is definitely the maximum size HTV-2 model which can be tested in X2, even if the physical sizing of the X2 facility would allow a larger model to used.

In some sense the result is promising as it shows that X2 should have the test time to study windward flow phenomena on a scaled HTV-2 vehicle such as convective heat flux, but probably not to study anything which requires the wake to be started, which may affect the ability to perform measurements such as free-flying model based force measurements which may require the wake to be started to be performed correctly.

Testing X2 scale models in larger expansion tubes such as UQ's X3 facility [86], HYPULSE [87] or LENS-XX [88], which all have test times of the order of a millisecond, would allow the 10s of flow lengths required to start the leeward flow and for the test model to move more in the post-shock flow if this is required for model image tracking.

Another consideration, which is further summarised at the start of Section 4 of James et al. [98], is that in an expansion tube, the accelerator gas, which the shocked test gas pushes down the tube in front of it as it unsteadily expands into the acceleration tube, actually flows over the model *before* the experiment begins. As we have seen in our experiments on X2, and has also been noted by others in the literature, such as in [99], this accelerator gas flow seemingly makes the model start quicker than it might do otherwise. This is similar to the 'prior steady flow' technique of Mudford and Stalker [100–102] which fairly successfully used a 'prior steady flow' going through the nozzle, which was closed off before the real test flow arrived, to allow a nozzle to be put on the end of a non-reflected shock tube, allowing a non-reflected shock tunnel to work in the very short test times available from those facilities.

5.4. High Density Flow Issues - Wall Boundary Layer Transition and Thick Diaphragms

When expansion tubes are ran at high densities, there are two main things to be considered: the effect of boundary layer transition on the wall of the facility's acceleration tube on facility performance and the effect of the thicker secondary diaphragms needed to contain the shock tube fill condition on the test model and the test flow itself.

In an expansion tube, the wall boundary layer in the acceleration tube has been noted to result in attenuation of the acceleration tube shock, such as in Sakamoto et al. [103]. This is not generally considered for most X2 test conditions, as normally we test with acceleration tube fill pressures from 1 to 20 Pa, but for conditions considered here with acceleration tube fill pressures of 230 to 286 Pa, this may need to be considered in condition modelling.

In an expansion tube, a thin secondary diaphragm separates the test gas in the shock tube from the accelerator gas downstream. Theoretically, this diaphragm is instantly broken when the shock in the shock tube hits it and it instantly vaporises and has no effect on the flow at all. This is obviously not the case in reality, and in the real case, the test flow needs to punch through or accelerate the diaphragm before it can go past it, leading to a complicated interaction which causes one of the largest uncertainties in the generation of expansion tube test conditions. A large discussion of this can be found in Section 3.4 of James et al. [80], with the study by Furakawa et al. [104] who performed schlieren near the rupture of an expansion tube secondary diaphragm being a particularly useful paper to physically illustrate the concept. The solution to this on X2 currently is just to use as thin of a secondary diaphragm as possible, to minimise its effect on the flow. Mylar diaphragms down to 2 µm are used on X2 for this purpose. However, these diaphragms can only hold a pressure difference of several kilopascals, meaning they would not be appropriate for high pressure conditions like the ones considered here which have shock tube fill pressures from 94 to 210 kPa (see Table 3). Considering Figure M.1 of Gildfind [105], where static rupture pressures of high pressure X2 secondary diaphragms are tested mylar secondary diaphragm thicknesses of 25 to 50 µm would be needed to hold the required pressures here, more than 10 times thicker than 2 µm. While the related post-shock pressures which hit the diaphragms will also be much larger, this may have a larger inertial effect on the flow, and heavy diaphragm fragments will travel down the tube after the experiment and potentially cause damage to the model and sensors mounted on it, which is a persistent issue in expansion tubes, even with thinner secondary diaphragms.

5.5. a_3 / a_2 Ratio Requirements

After the first large treatise on expansion tubes by Trimpi in 1962 [106], the expansion tube was considered a promising new facility type and many prototype facilities were built. However, it was always found to be difficult to generate reliable conditions in the machines due to unknown issues causing excessive noise on the measurements. In 1992 Paull and Stalker [107] found that noise from the primary diaphragm rupture in an expansion tube was transferred to the test gas in the shock tube, across the shocked test gas (state 2) and unsteadily expanded driver gas (state 3) interface, which was then focused into particular frequencies by the unsteady expansion process in the acceleration tube, resulting in a corrupted test flow. By running the facility in a way which ensured that the sound speed of the shocked test gas (a_2) was greater than the second speed of the unsteadily expanded driver gas (a_3) behind it, it was posited that this could be avoided. If defined as the a_2 / a_3 ratio, this means that a_2 / a_3 should be greater than 1 to ensure that this noise is not transmitted. Using this principle, expansion tubes have become a major and important hypersonic test facility type around the world, with their use

generally skewed towards the high end of their performance envelope as this generally ensures that a_2 / a_3 is greater than 1.

If we want to study these boost-glide conditions in X2, we need to consider whether this rule can be relaxed slightly to allow slower conditions to be generated. Fig. 8 shows the sound speed ratio for all of the potential conditions from Table 3. Considering the results shown in the figure, it can be seen that none of the driver conditions meet the Paull and Stalker criterion of a_2 / $a_3 > 1$, however, there is some variation, caused by the amount of helium and argon in the different driver conditions. Two of the driver conditions (x2-lwp-2.0-100He-0 and x2-lwp-2.5-100He-0) use pure helium driver gases, to increase performance, so they have very high unsteadily expanded driver gas sound speeds. For the three 2.5 mm diaphragm thickness driver conditions (x2-lwp-2.5-0, x2-lwp-2.5-90He-0, and x2-lwp-2.5-100He-0), which are higher performance due to their higher compression ratio, the condition with a driver composition of 80%He/20%Ar (by volume) [108], has the lowest sound speed ratio, so in the end, it may end up being the best test condition to continue with, if this ratio is the most important criterion.

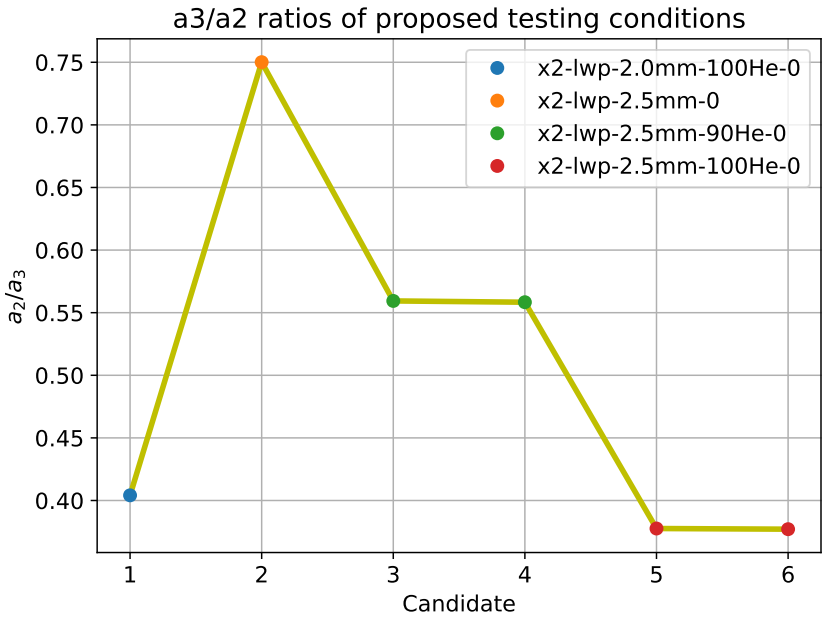

Fig 8. a_2/a_3 ratios for the proposed test conditions.

As all of these conditions fail to meet this criterion, the consideration is then whether this criterion sufficiently encapsulates all of the physical phenomena involved in making an expansion tube test condition good or bad. For example, in the authors' experience, almost every condition tested on X2 with a CO_2 (or predominantly CO_2) test gas does not fulfill this criterion, due to the reduced γ and high molecular weight of CO_2. However, many of these conditions appear to be good quality, so while this criterion is important and something to keep in mind and be wary of, as many expansion tube conditions were low quality before this criterion was proposed, further experimental testing is required to ascertain the quality of the test conditions proposed in this paper.

5.6. Required Mach number - More Expansion or Bigger Nozzles?

As mentioned in Section 4, for the conditions where the test flow achieves the desired velocity and density of the HTV-2 B flight, their Mach numbers are lower than that of the actual flight case. This is because it is generally not possible in an expansion tube to unsteadily expand the flow back to the real flight freestream temperature, and instead, the test flow is generated with an elevated freestream temperature which consequently drops the flow Mach number. In regular expansion tube operation, the inability to reach higher Mach numbers is generally not an issue, thanks to the Oswatitsch's Mach number

independence principle [109], which states that at high Mach numbers, non-dimensional aerodynamic quantities (such as pressure coefficient, lift, flowfield structure, and shock wave shapes) become independent of the Mach number. However, this principle is more applicable to blunt-body objects, which are the usual test models used in expansion tubes, as opposed to the slender body of a boost-glide vehicle. This is due to the fact that Mach number M_∞ frequently appears in combined form $M_\infty^2 \sin^2 \beta$ in equations for various important parameters (such as the post-shock pressure ratio) of the test model, where β is the shock wave angle, which is large for blunt bodies but small for slender bodies [52]. Tsien [110] had an earlier similarity law for slender hypersonic flows which relied on the product of the flow Mach number (M_∞) and a body thickness ratio ($\tau = \frac{\delta}{b}$ with Tsien defining $2b$ as the length of the body and δ as the thickness of the body [110]) being approximately 1 i.e. $M_\infty \tau \approx 1$. As stated by Oswatitsch himself [109], Tsien's slender body similarity law [110] does not allow the Mach number to go to infinity without the body shape changing. To maintain the $M_\infty \tau \approx 1$ as $M_\infty \to \infty$ also needs $\tau \to 0$, which will not work if we hope maintain the geometry of the vehicle. This seemingly implies that slender body flows will require simulation at the exact flight Mach number. The requirement for the $M_\infty \tau$ product to be conserved also popped up in Section 5.2 where the discussion of binary scaling for slender bodies was discussed, which seems to be something else pointing the to the fact that the Mach number needs to be re-created to simulate slender hypersonic flows.

The question then is how blunt does an object have to be to be Mach number independent? This is examined in Fig. 9 where the flight freestream condition for the HTV-2 B flight was taken from Table 1 and the post-shock density was scaled by a factor of 20 and then we looped through a freestream temperature range from the actual flight freestream temperature to 3.5 times the flight freestream temperature to change the flow Mach number, M_8 by convention for an X2 condition with the nozzle on, from the flight Mach number of 18.43 to around Mach 10, the design point of X2's nozzle. To ensure that the flow stagnation enthalpy (H_t) was constant, the chemical enthalpy of the freestream state was calculated with CEA and then removed from Ht to find the correct freestream velocity for each case to ensure $v_8 + h_8 = H_t$ for every case. An equilibrium wedge shock was then performed for each AoA at each case and stitched together to produces curves of the effect of M_8 on each AoA over our AoA range from 0 to 30° from Section 3 (which gives a wedge angle range from 3.43 to 33.43°.

Examining Fig. 9a, where the Mach number is plotted against the wedge shock angle (β) minus the wedge angle (θ) to make it easier to compare different AoA values, it can be seen that as the AoA gets larger the change in $\beta - \theta$ with Mach number gets weaker. For an AoA of 0° the change with Mach number is very pronounced across the whole Mach number range, with almost a 50% reduction in $\beta - \theta$ over the whole range. For higher AoA values such as 20° and above, the change in $\beta - \theta$ with Mach number is very slight above around Mach 15, and the change in slope between individual AoA values appear to have stopped above 20° as well, potentially indicating that above 20° AoA the flow has become as independent of Mach number as possible for a non-blunted geometry.

Similar results are seen when we consider normalised post-shock pressure, density and temperature in Figs. 9b, 9c, 9d. At low AoA values again, large changes are seen across the Mach number range with a 50% drop in post-shock pressure over the whole range, a 40% decrease in post-shock density, and a 60% decrease in post-shock temperature at an AoA of 0°. Once again, these changes get less pronounced as AoA increases, and for the post-shock pressure especially (Fig. 9b) for AoA of 20° and above, the flow appears to be almost Mach number independent. While this is not so true for the post-shock density and temperature, they still do appear to be fairly Mach number independent for AoA values of 20° and above and Mach numbers above 15, similar to what was seen for the $\beta - \theta$ in Fig. 9a. The post-shock temperature appears to be effectively constant above Mach 15 in Fig. 9d and Fig. 9d the degree of increase in density is with Mach number is very small above Mach 15.

Considering the Candidate conditions in Table 3 it can be seen that conditions with the x2-lwp-2.5mm-100He-0 driver condition are the only ones to theoretically have a Mach number greater than 15, however, x2-lwp-2.0mm-100He-0 and x2-lwp-2.5mm-90He-0 driver conditions are close with Mach numbers of around 14, where the curves are still fairly flat in Fig. 9. This shows that potential conditions are available where the flow will be fairly Mach number independent if large AoA values above 20° are used.

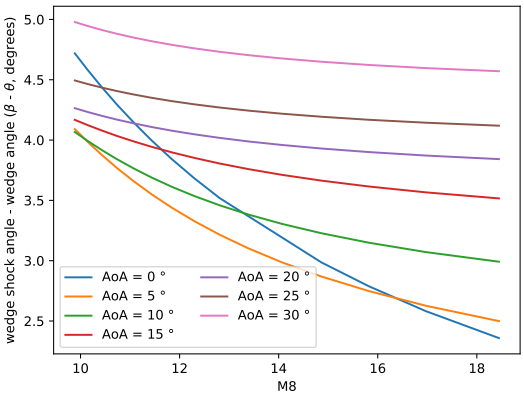

(a) effect of M_8 on the oblique shock angle - wedge angle ($\beta - \theta$)

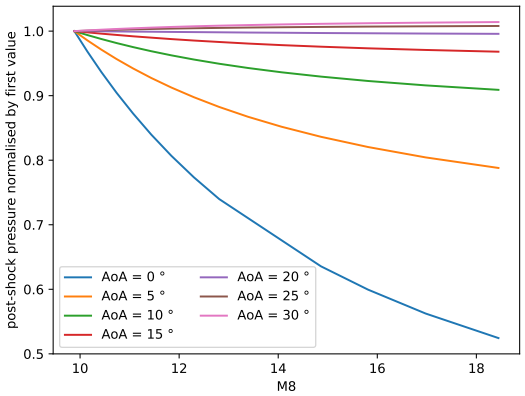

(b) effect of M_8 on post-shock pressure

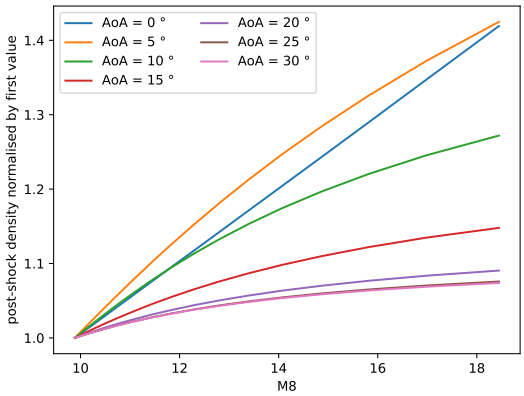

(c) effect of M_8 on post-shock density

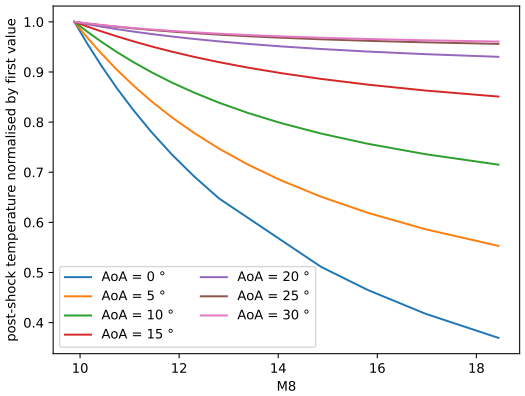

(d) effect of M_8 on post-shock temperature

Fig 9. The effect of flow Mach number in the facility (M_8) on equilibrium gas properties over the model, which is simulated by a wedge at different angles of attack.

If lower AoA values need to be tested, then either testing will have to be done at a lower Mach number and analysis such as simulating the experiments will have to be done to interpret the results compared to a flight case. Potentially different conditions from Table 3 could be tested, to observe the effect of having different Mach numbers on the performance of the HTV-2 model. It may be possible to predict the results at the flight Mach number by simple interpolation, or it may be reasonable to conclude that the higher Mach number tests are effective representations of the peak heating point of the actual flight, if the results show good convergence.

If higher Mach number than the conditions in Table 3 are required, there are some options. The first option is to promote more unsteady expansion in the acceleration tube, by shocking the test gas less and unsteadily expanding it further, to achieve a higher nozzle entrance Mach number, and as such, a higher nozzle exit Mach number. This has two potential issues. Firstly, the nozzle is designed for an entrance Mach number of 7.3, and while it is quite robust generally, most of the Candidate conditions in Table 3 are already well above this value, and potentially at some point the nozzle will no longer work as it should. The simulations from Table 4 were already performed using the nozzle's geometric area ratio of 5.64 which in reality is sometimes lower due to boundary layer growth in the acceleration

tube before the flow enters the nozzle and further boundary layer growth in the nozzle itself, which is discussed further in Section 3.6 of James et al. [80]. Secondly, from our experience most X2 conditions work best with a v_{s1}/v_{s2} ratio of 0.5, which means the shock speed in the shock tube is half that of the acceleration tube, and some conditions actually work better when it is slightly greater than 0.5, meaning more shock in the shock tube and less unsteady expansion in the acceleration tube, as was seen in Curtis et al. [111]. In that work conditions seemed less steady when the v_{s1}/v_{s2} ratio was less than 0.5, as all of the conditions in Table 3 are. So if we expand the flow further, v_{s1}/v_{s2} will drop further, but it is worth trying if the Mach number is needed. The final issue is finding a driver condition to use, as it seems that with decreasing v_{s1}/v_{s2} ratios, higher performance driver conditions are needed as the highest Mach number conditions are also the conditions with the lowest v_{s1}/v_{s2} values but they're already using X2's most powerful current driver condition (x2-lwp-2.5mm-100He-0), which is a pure helium driver with a compression ratio of 40 [108]. Potentially higher compression ratio driver conditions would allow conditions to be simulated at the flight Mach number.

The second option is to use a facility nozzle with a larger area ratio. X2's nozzle has an area ratio of 5.64 and is designed for inflow and exit Mach numbers of 7.3 and 10 respectively [79]. This is quite a common expansion tube nozzle geometry as it has been copied for UQ's X3 facility [112] and also Oxford T6 multi-mode expansion tube facility [113]. Utilising a larger area ratio nozzle would allow the test flow to expand more, thus dropping the test flow temperature and sound speed, which leads to a higher Mach number. Several expansion tubes do in fact have larger area ratio nozzles. X3 also has a nozzle with an area ratio of 9.86 with design inlet and exit Mach numbers of 7.48 and 12 respectively [114], which during experimental commissioning measurements of the shock angle over a wedge model, was found to have a Mach number of 11 ± 0.9 [115]. HYPULSE has an even larger area ratio nozzle with an area ratio of 16, which was designed for an inlet Mach number of 7.5 and also has an exit Mach number of 12. While the LENS-XX nozzle geometry is not public, some of their papers, such as MacLean et al. [116], quote test flow Mach numbers up to 18, so they clearly have a big nozzle too. A similar nozzle to one of these nozzles could be used on X2 to get the Mach number up, but due to the effort and expense of designing, building, and commissioning a new facility nozzle, potentially X3 or HYPULSE may just be better places to test these conditions, even if their nozzles may not work optimally to generate higher Mach number flows if their inlet Mach number is raised.

5.7. Nozzle or No Nozzle

When expansion tubes need to be operated at the edge of their performance envelopes, which will be true for most facilities trying to study scaled boost-glide re-entry conditions, an option to generate even more $\rho \cdot L$ product for scaled experimentation is to run the facility without a nozzle. This means that the test models get even smaller, and the scaling factors larger, but generally more density is lost through the nozzle expansion than is gained in physical scale, meaning that the nozzle reduces the achievable $\rho \cdot L$ product. For example, X2's nozzle generally reduces the flow density by an order of magnitude, but the model scale only increases by around a factor of 2, so the achievable $\rho \cdot L$ is reduced by a factor of 5 with the nozzle.

As alluded to above, the issue here is that the models will get even smaller, and the Mach number will be even lower due to not having a nozzle to expand the flow to higher Mach numbers. So this may be something which is more appropriate for larger facilities such as X3. The X3 caret waverider study [55] was performed in X3 at Mach 10 without a nozzle, for example.

5.8. Test Flow Chemical Freezing

Any test facility which shocks a gas to a high temperature and then rapidly expands it to generate a test flow has some uncertainty in how much of the test gas will recombine in this expansion process. While this is less of an issue in expansion tubes than it is in shock tunnels, due to the test gas never being stagnated at full total pressure, it can still be an issue, as the gas is still shocked quite strongly in the shock tube, before it is unsteadily expanded in the acceleration tube and then steadily expanded in the nozzle.

As mentioned in Section 5.6, shocking the test gas less in the shock tube and unsteadily expanding the gas more in the acceleration tube is an option for pursuing a lower test flow temperature, and thereby

a lower speed of sound and higher Mach number. It is unclear whether this will cause more severe chemical freezing, as the maximum temperature will be lower, but the test gas will be expanded by a larger factor.

The other issue here is that the test model is not a blunt body and for blunt body flows any non-equilibrium in the test flow is believed to have little effect on the post-shock flow because the bow shock on a blunt body is so strong that it will quite quickly remove the history of the any test flow non-equilibrium from the resultant post-shock flow. With a non-blunt test model, the conditions behind the oblique shock over the model will be much weaker, so there is the potential that the post-shock chemistry over the test model may be affected by any flow non-equilibrium which does occur.

Ignoring a reflected shock off the secondary diaphragm, which can doubly shock the test gas, the worst case scenario for the chemical freezing is that the test gas is dissociated behind the shock in the shock tube and then does not recombine at all in the acceleration tube and nozzle, meaning that this is the chemical state which flows over the test model. Considering Candidate condition 6 from Table 3 as an example condition, the post-shock composition in the shock tube at equilibrium is shown in Table 4 below. It can be seen that there is very little oxygen and nitrogen dissociation of the gas, even though it is quite vibrationally excited (γ_2 is 1.22). There is minor but appreciable NO formation.

Table 4. Equilibrium post-shock composition in the shock tube (state 2) for Candidate condition 6 from Table 3 ignoring trace species.

Species	Mole fraction
O_2	0.185
O	4.23×10^{-3}
N_2	0.766
N	1.123×10^{-6}
NO	45.2×10^{-3}

To compare the post-shock composition in the shock tube from Table 4 to the equilibrium conditions behind the shock over a potential HTV-2 model, the freestream conditions for Candidate condition 6 from Table 3 were used to generate Fig. 10 below which shows the post-shock equilibrium composition behind a wedge for different AoA values. It can be seen that oxygen dissociation and NO production begin at an AoA of around $10°$. This means that if the test gas is fully frozen from its post-shock state in the shock tube up to the test model and the AoA is less than $10°$, there is a risk that the post-shock flow will be more dissociated than it would be otherwise, but above that AoA, it would just mean that this chemistry was done before reaching the shock, instead of after it.

6. Conclusions

This paper evaluated the feasibility of testing boost-glide vehicles in UQ's X2 expansion tube on a theoretical level, by examining the required model scaling factor for the HTV-2 vehicle in X2, and identifying suitable test conditions through conducting simulations using UQ's PITOT3 equilibrium gas expansion tube simulation code. It was found that the peak heating point of the HTV-2 vehicle, which occurs at the altitude of 49.01 km where the vehicle travels at 6080 m/s, can be seemingly tested in our X2 facility at 1:20 scale. This can be achieved with multiple potential conditions. There are some unique issues to manage such as the effects of large scaling factors, test time limitatons, high density flows, generated the required flow Mach number, and test flow chemical freezing, but we are confident adequate testing could be performed.

Future work to investigate this topic will include time-resolved CFD simulations of the proposed conditions, experimental testing of the conditions on the facility to ascertain their quality, before final conditions are designed, and considerations of how other expansion tubes such as UQ's larger X3 facility and cold driven or detonation driven expansion tubes could be used to generate these conditions. The end goal is to eventually test boost-glide vehicles in X2 to measure heat flux, pressure loading, forces and

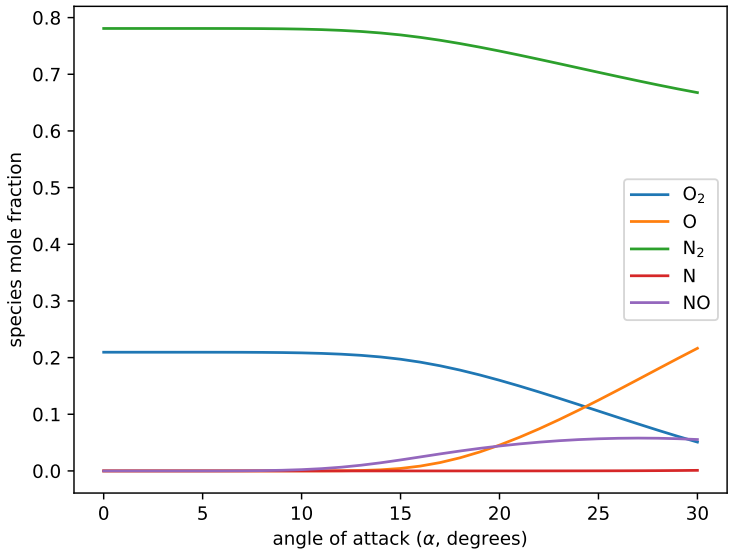

Fig 10. The effect of angle of attack on the equilibrium post-wedge-shock composition for Candidate condition 6 from Table 3 ignoring trace species.

moments, and optical measurements such as schlieren and emission spectroscopy of the species in the post-shock flow.

There are also some more generic and interesting paths of enquiry which came out of the consideration of the unique characteristics of the types of conditions which also deserve further enquiry, such as how much of the wake flow of a vehicle needs to be started for free-flight force measurements to be valid, whether the Paull and Stalker [107] a_2/a_3 ratio is true in all cases or if sometimes other phenomena comes into play, how blunt does a test model need to be to be considered Mach number independent, why such a powerful facility driver is required to generate the required conditions at the flight Mach number, and finally, why do most good expansion tube conditions seem to have an acceleration tube shock speed which is around double the shock tube shock speed. These questions are all tangential to the current work, but progress in these areas would help pushing this work, and all other expansion work, forward.

References

[1] Sänger, E., *Raketen-Flugtechnik*, R. Oldenbourg, Munich and Berlin, 1933. Translated into English as Rocket Flight Engineering, NASA Technical Translation F-223, 1965.

[2] Sänger, E., and Bredt, I., *A Rocket Drive for Long Range Bombers*, Bureau of Aeronautics, Navy Department, Trans. CGD-32, 1944.

[3] Seiff, A., and Allen, H., *Some aspects of the design of hypersonic boost-glide aircraft*, NACA Ames Aeronautical Laboratory, Moffett Field, Calif., U.S.A., 1955.

[4] Eggers, A. J., "Performance of Long Range Hypervelocity Vehicles," *Journal of Jet Propulsion*, Vol. 27, No. 11, 1957, pp. 1147–1151. doi:10.2514/8.12488.

[5] Eggers, A., Allen, H., and Neice, S., *A comparative analysis of the performance of long-range hypervelocity vehicles, NACA Report 1382*, NACA Ames Aeronautical Laboratory, Moffett Field, Calif., U.S.A., 1958.

[6] Cornog, R., "Some Economic Aspects of Hypersonic Flight," *ARS Journal*, Vol. 29, No. 10, 1959, pp. 706–715. doi:10.2514/8.4878.

[7] Ashford, D. M., "Boost-Glide Vehicles for Long Range Transport," *The Journal of the Royal Aeronautical Society*, Vol. 69, No. 655, 1965, pp. 448–458. doi:10.1017/s000192400005908x.

[8] Hunter, M., and Fellenz, D., "The Hypersonic Transport-The Technology and the Potential," *AIAA 7th Annual Meeting and Technical Display, Houston, TX*, 1970.

[9] Krieger, R. J., "Supersonic missile aerodynamic and performance relationships for long-range mission profiles," *Journal of Spacecraft and Rockets*, Vol. 21, No. 3, 1984, pp. 234–240. doi: 10.2514/3.25643.

[10] Li, Y., and Cui, N.-g., "Maximum crossrange for hypersonic boost-glide missile," *2008 2nd International Symposium on Systems and Control in Aerospace and Astronautics*, IEEE, 2008. doi: 10.1109/isscaa.2008.4776361.

[11] Rizvi, S., Linshu, H., Dajun, X., and Shah, S., "Trajectory optimisation for a rocket-assisted hypersonic boost-glide vehicle," *The Aeronautical Journal*, Vol. 121, No. 1238, 2017, pp. 469–487. doi:10.1017/aer.2017.11.

[12] Acton, J. M., "Hypersonic Boost-Glide Weapons," *Science & Global Security*, Vol. 23, No. 3, 2015, pp. 191–219. doi:10.1080/08929882.2015.1087242.

[13] Wright, D., "Research Note to Hypersonic Boost-Glide Weapons by James M. Acton: Analysis of the Boost Phase of the HTV-2 Hypersonic Glider Tests," *Science & Global Security*, Vol. 23, No. 3, 2015, pp. 220–229. doi:10.1080/08929882.2015.1088734.

[14] Tracy, C. L., and Wright, D., "Modeling the Performance of Hypersonic Boost-Glide Missiles," *Science & Global Security*, Vol. 28, No. 3, 2020, pp. 135–170. doi:10.1080/08929882.2020. 1864945.

[15] Lunan, D. A., "Waverider, a revised chronology," *20th AIAA International Space Planes and Hypersonic Systems and Technologies Conference*, Glasgow, Scotland, July 6-9, 2015.

[16] Rasmussen, M. L., "Waverider Configurations Derived from Inclined Circular and Elliptic Cones," *Journal of Spacecraft and Rockets*, Vol. 17, No. 6, 1980, pp. 537–545. doi:10.2514/3.57771.

[17] Rasmussen, M. L., and Clement, L. W., "Cone-derived waveriders with longitudinal curvature," *Journal of Spacecraft and Rockets*, Vol. 23, No. 5, 1986, pp. 461–469. doi:10.2514/3.25830.

[18] Bowcutt, J. D. . C. D., K. G. & Anderson, "Viscous optimized hypersonic waveriders," *25th AIAA Aerospace Sciences Meeting*, American Institute of Aeronautics and Astronautics, 1987. doi: 10.2514/6.1987-272.

[19] Anderson, J. D., Lewis, M. J., Kothari, A. P., and Corda, S., "Hypersonic waveriders for planetary atmospheres," *Journal of Spacecraft and Rockets*, Vol. 28, No. 4, 1991, pp. 401–410. doi: 10.2514/3.26259.

[20] Lewis, M. J., and McRonald, A. D., "Design of hypersonic waveriders for aeroassisted interplanetary trajectories," *Journal of Spacecraft and Rockets*, Vol. 29, No. 5, 1992, pp. 653–660. doi: 10.2514/3.11506.

[21] O'Neill, M. K. L., and Lewis, M. J., "Design tradeoffs on scramjet engine integrated hypersonic waverider vehicles," *Journal of Aircraft*, Vol. 30, No. 6, 1993, pp. 943–952. doi:10.2514/3.46438.

[22] Tincher, D. J., and Burnett, D. W., "Hypersonic waverider test vehicle - A logical next step," *Journal of Spacecraft and Rockets*, Vol. 31, No. 3, 1994, pp. 392–399. doi:10.2514/3.26451.

[23] Heinze, W., and Bardenhagen, A., "Waverider Aerodynamics and Preliminary Design for Two-Stage-to-Orbit Missions, Part 2," *Journal of Spacecraft and Rockets*, Vol. 35, No. 4, 1998, pp. 459–466. doi:10.2514/2.3376.

[24] Strohmeyer, D., Eggers, T., and Haupt, M., "Waverider Aerodynamics and Preliminary Design for Two-Stage-to-Orbit Missions, Part 1," *Journal of Spacecraft and Rockets*, Vol. 35, No. 4, 1998, pp. 450–458. doi:10.2514/2.3375.

[25] O'Brien, T. F., and Lewis, M. J., "Rocket-Based Combined-Cycle Engine Integration on an Osculating Cone Waverider Vehicle," *Journal of Aircraft*, Vol. 38, No. 6, 2001, pp. 1117–1123. doi:10.2514/2.2880.

[26] Ragnoli, G., Savino, R., Cecere, A., and Rigamonti, M., "Hypersonic Boost-Glide Systems: flight mechanics and plasma parameters evaluation through aero-thermo-chemical computational fluid dynamics," *Aerospace Science and Technology*, 2024, p. 109092. doi:10.1016/j.ast.2024.109092.

[27] Hui, X., Guangbin, C., Shengxiu, Z., Xiaogang, Y., and Mingzhe, H., "Hypersonic reentry trajectory optimization by using improved sparrow search algorithm and control parametrization method," *Advances in Space Research*, Vol. 69, No. 6, 2022, pp. 2512–2524. doi:10.1016/j.asr.2021.12.030.

[28] Chen, Y., Zheng, H., Ren, X., He, B., Dong, C., Cai, G., and Liu, L., "Backward Monte Carlo method for simulating spectral radiation characteristics of boost-gliding vehicle," *Aerospace Science and Technology*, Vol. 132, 2023, p. 108087. doi:10.1016/j.ast.2022.108087.

[29] Rataczak, J. A., Chaudhry, R. S., McMahon, J. W., and Boyd, I. D., "Investigation of Surface-Catalycity Effects on Hypersonic Glide Vehicle Trajectory Optimization," *Journal of Spacecraft and Rockets*, 2024, pp. 1–13. doi:10.2514/1.a35764.

[30] Rataczak, J. A., McMahon, J. W., and Boyd, I. D., "Reachability Analysis of a Hypersonic Glide Vehicle using Particle Swarm Optimization," *AIAA SCITECH 2023 Forum*, American Institute of Aeronautics and Astronautics, 2023. doi:10.2514/6.2023-1172.

[31] Williams, D., Bartkowicz, M., and Candler, G. V., "Shape Optimization for a Parametrically-Defined Hypersonic Glide Vehicle," *AIAA SCITECH 2024 Forum*, American Institute of Aeronautics and Astronautics, 2024. doi:10.2514/6.2024-0562.

[32] Candler, G. V., and Leyva, I. A., "Computational Fluid Dynamics Analysis of the Infrared Emission From a Generic Hypersonic Glide Vehicle," *Science & Global Security*, Vol. 30, No. 3, 2022, pp. 117–130. doi:10.1080/08929882.2022.2145777.

[33] Tracy, C. L., and Wright, D., ""Computational Fluid Dynamics Analysis of the Infrared Emission from a Generic Hypersonic Glide Vehicle"—A Response," *Science & Global Security*, Vol. 31, No. 1–2, 2023, pp. 41–47. doi:10.1080/08929882.2023.2215587.

[34] Zou, S., Candler, G. V., Yang, S., Carr, Z. R., Portoni, P., Zelasko, T., and Wadhams, T. P., "Computational and experimental investigation of near-field sonic boom of a HTV-2 type hypersonic boost gliding vehicle," *AIAA SCITECH 2024 Forum*, American Institute of Aeronautics and Astronautics, 2024. doi:10.2514/6.2024-0671.

[35] Gottlieb, J. R., Mines, J. M., Garmendia, D. C., Emhoff, J. W., and Clemens, D. E., "Coupled Vehicle and Trajectory Design Optimization for Boost-Glide Hypersonic Systems," *AIAA SCITECH 2024 Forum*, American Institute of Aeronautics and Astronautics, 2024. doi:10.2514/6.2024-0373.

[36] Rodi, P. E., "Effects of Finite Radius Leading Edges on the Performance of Capsule/Waveriders for Boost-Glide Missions," *AIAA AVIATION 2022 Forum*, American Institute of Aeronautics and Astronautics, 2022. doi:10.2514/6.2022-4050.

[37] Shi, H., Niu, Z., Hun, L., Zhang, P., Wang, F., and Zhao, L., "A Full-trajectory Design Method for a Waverider Hypersonic Vehicle with Boost-glide-attack Process," *2023 38th Youth Academic Annual Conference of Chinese Association of Automation (YAC)*, IEEE, 2023. doi:10.1109/yac59482.2023.10401454.

[38] Walker, S., Sherk, J., Shell, D., Schena, R., Bergmann, J., and Gladbach, J., "The DARPA/AF Falcon Program: The Hypersonic Technology Vehicle #2 (HTV-2) Flight Demonstration Phase," *15th AIAA International Space Planes and Hypersonic Systems and Technologies Conference*, American Institute of Aeronautics and Astronautics, 2008. doi:10.2514/6.2008-2539.

[39] Williamson, J., and Wirtz, J. J., "Hypersonic or just hype? Assessing the Russian hypersonic weapons program," *Comparative Strategy*, Vol. 40, No. 5, 2021, pp. 468–481. doi:10.1080/01495933.2021.1962198.

[40] Kessler, A., "Russian Hypersonic Glide Vehicles: What to Know and What to Fear," *Orbis*, Vol. 66, No. 2, 2022, pp. 213–223. doi:10.1016/j.orbis.2022.02.009.

[41] Bugos, S., "China Tested Hypersonic Capability, US Says," *Arms Control Today*, Vol. 51, No. 9, 2021, pp. 19–20.

[42] Brookes, P., and Venable, J., "Chinese Hypersonic Weapons Developments Must Be Countered," 2021.

[43] Winter, M. W., McDaniel, R. D., Chen, Y.-K., Saunders, D., and Jenniskens, P., "Radiation Modeling for Reentry of Hayabusa Sample Return Capsule," *Journal of Spacecraft and Rockets*, Vol. 56, No. 4, 2019, pp. 1152–1164. doi:10.2514/1.a34381.

[44] Bakos, R., and Erdos, J., "Options for enhancement of the performance of shock-expansion tubes and tunnels," *33rd AIAA Aerospace Sciences Meeting and Exhibit*, Reno, NV, U.S.A., January 9-12, 1995.

[45] Itoh, K., "Characteristics of the HIEST and its Applicability for Hypersonic Aerothermodynamic and Scramjet Research," *Progress in Astronautics and Aeronautics*, edited by F. Lu and D. Marren, AIAA, 2002, Chap. 10, pp. 279–314. doi:https://doi.org/10.2514/5.9781600866678.0279.0314.

[46] Bray, K. N. C., "Atomic recombination in a hypersonic wind-tunnel nozzle," *Journal of Fluid Mechanics*, Vol. 6, No. 1, 1959, pp. 1–32. doi:10.1017/S0022112059000477.

[47] Park, C., "Thermochemical relaxation in shock tunnels," *Journal of Thermophysics and Heat Transfer*, Vol. 20, No. 4, 2006, pp. 689–698. doi:10.2514/1.22719.

[48] Stalker, R., "Isentropic Compression of Shock Tube Driver Gas," *ARS Journal*, Vol. 30, 1960, p. 564.

[49] Gildfind, D., Morgan, R. G., and Jacobs, P., "Expansion Tubes in Australia," *Experimental Methods of Shock Wave Research*, edited by O. Igra and F. Seiler, Springer, 2016, pp. 399–431. doi:10.1007/978-3-319-23745-9_13.

[50] Collen, P., Doherty, L. J., Subiah, S. D., Sopek, T., Jahn, I., Gildfind, D., Geraets, R. P., Gollan, R., Hambidge, C., Morgan, R., and McGilvray, M., "Development and commissioning of the T6 Stalker Tunnel," *Experiments in Fluids*, Vol. 62, No. 11, 2021. doi:10.1007/s00348-021-03298-1.

[51] Tanno, H., Komuro, T., Sato, K., Itoh, K., Arai, K., and Yamada, K., "Basic characteristics of the free-piston driven expansion tube JAXA HEK-X," *32nd AIAA Aerodynamic Measurement Technology and Ground Testing Conference*, Washington, D.C., U.S.A., June 13-17, 2016.

[52] Anderson, J. D., *Hypersonic and high-temperature gas dynamics*, 2nd ed., American Institute of Aeronautics and Astronautics, Reston, Va, 2006.

[53] Gibson, W. E., and Marrone, P. V., "Chapter 6 - A Similitude for Non-Equilibrium Phenomena in Hypersonic Flight," *The High Temperature Aspects of Hypersonic Flow*, AGARDograph, Vol. 68, edited by W. C. Nelson, Elsevier, 1964, pp. 105–131. doi:https://doi.org/10.1016/B978-1-4831-9828-6.50011-4.

[54] Ellington, D., "Binary scaling limits for hypersonic flight," *AIAA Journal*, Vol. 5, No. 9, 1967, pp. 1705–1706. doi:\href{https://doi.org/10.2514/3.4284}{10.2514/3.4284}.

[55] Silvester, T. B., McIntyre, T. J., and Morgan, R. G., "Superorbital expansion tube tests of a caret waverider," *Shock Waves*, Vol. 17, No. 1, 2007, pp. 51–63. doi:\href{http://dx.doi.org/10.1007/s00193-007-0100-3}{10.1007/s00193-007-0100-3}.

[56] Angelini, R., and Denaro, A., "IXV re-entry demonstrator: Mission overview, system challenges and flight reward," *Acta Astronautica*, Vol. 124, 2016, pp. 18–30. doi:10.1016/j.actaastro.2016.02.015.

[57] Vella, S., "Expansion Tunnel Heat Transfer Measurements of the ESA-IXV Re-entry Vehicle," Bachelor of engineering thesis, the University of Queensland, St Lucia, Australia, 2016.

[58] Wallington, J., and James, C., "Testing a free flying model of the ESA IXV in the X2 expansion tube," *23rd Australasian Fluid Mechanics Conference*, Sydney, Australia, December 4-8, 2022.

[59] Wallington, J., "Free flying ESA-IXV in the X2 Expansion tube," Bachelor of engineering thesis, the University of Queensland, St Lucia, Australia, 2022.

[60] Gillum, M., Kammeyer, M., and Burnett, D., "Wind tunnel results for a Mach 14 waverider," *32nd Aerospace Sciences Meeting and Exhibit*, Reno, NV, U.S.A., June 10-13, 1994.

[61] Gillum, M., Kammeyer, M., and Burnett, D., "Details of a Mach 14 waverider wind tunnel test," *18th AIAA Aerospace Ground Testing Conference*, Colorado Springs, CO, U.S.A., June 20-23, 1994.

[62] Gillum, M. J., and Lewis, M. J., "Experimental Results on a Mach 14 Waverider with Blunt Leading Edges," *Journal of Aircraft*, Vol. 34, No. 3, 1997, pp. 296–303. doi:10.2514/2.2198.

[63] Miller, R., Argrow, B., Center, K., Brauckmann, G., and Rhode, M., "Experimental verification of the osculating cones method for two waverider forebodies at Mach 4 and 6," *36th AIAA Aerospace Sciences Meeting and Exhibit*, Reno, NV, U.S.A., January 12-15, 1998.

[64] Norris, J., "Mach 8 high Reynolds number static stability capability extension using a hypersonic waverider at AEDC tunnel 9," *25th AIAA Aerodynamic Measurement Technology and Ground Testing Conference*, San Francisco, CA, U.S.A., June 5-8, 2006.

[65] Liu, J.-x., Hou, Z.-x., Chen, X.-q., and Zhang, J.-t., "Experimental and numerical study on the aero-heating characteristics of blunted waverider," *Applied Thermal Engineering*, Vol. 51, No. 1–2, 2013, pp. 301–314. doi:10.1016/j.applthermaleng.2012.09.026.

[66] Liu, J.-x., Hou, Z.-x., Ding, G.-h., Chen, X.-q., and Chen, X.-q., "Numerical and experimental study on waverider with blunt leading edge," *Computers & Fluids*, Vol. 84, 2013, pp. 203–217. doi:10.1016/j.compfluid.2013.06.005.

[67] Lobbia, M. A., and Suzuki, K., "Experimental Investigation of a Mach 3.5 Waverider Designed Using Computational Fluid Dynamics," *AIAA Journal*, Vol. 53, No. 6, 2015, pp. 1590–1601. doi:10.2514/1.j053458.

[68] Chuanzhen, L., Xufei, M., Rongjian, L., and Peng, B., "Experimental and numerical investigation for hypersonic performance of double swept waverider," *Acta Astronautica*, Vol. 200, 2022, pp. 291–300. doi:10.1016/j.actaastro.2022.08.004.

[69] Liu, C., Liu, R., Meng, X., and Bai, P., "Experimental Investigation on Off-Design Performances of Double-Swept Waverider," *AIAA Journal*, Vol. 61, No. 4, 2023, pp. 1596–1607. doi:10.2514/1.j062254.

[70] Nasa Oceanic and Atmospheric Administration, National Aeronautics and Space Administration, United States Air Force, *U.S. Standard Atmosphere, 1976, NOAA-S/T 76-1562*, Nasa Oceanic and Atmospheric Administration, Washington, D.C., U.S.A., 1976.

[71] Griffin, M. D., and French, J. R., *Space Vehicle Design*, 2nd ed., American Institute of Aeronautics and Astronautics, Reston, Va, 2004.

[72] Gollan, R.G. and Damm, K. and Gibbons, N. and Bond, D. and Jacobs, P.A., "GDTk - GDTk: Gas Dynamics Toolkit," https://gdtk.uqcloud.net/, 2022. Accessed March 10, 2022.

[73] Gordon, G., and McBride, B., *Computer Program for Calculation of Complex Chemical Equilibrium Compositions and Applications I. Analysis*, NASA Lewis Research Center, Cleveland, OH, U.S.A., 1994.

[74] McBride, B., and Gordon, G., *Computer Program for Calculation of Complex Chemical Equilibrium Compositions and Applications II. Users Manual and Program Description*, NASA Lewis Research Center, Cleveland, OH, U.S.A., 1996.

[75] Bui, T., "Testing of a Free-Flying Hypersonic Glider in an Expansion Tube," Bachelor of engineering thesis, the University of Queensland, St Lucia, Australia, 2023.

[76] Zhang, B., Feng, Z., Xu, B., and Yang, T., "Efficient Aerodynamic Shape Optimization of the Hypersonic Lifting Body Based on Free Form Deformation Technique," *IEEE Access*, Vol. 7, 2019, pp. 147991–148003. doi:10.1109/access.2019.2945082.

[77] Niu, Q., Yuan, Z., Chen, B., and Dong, S., "Infrared radiation characteristics of a hypersonic vehicle under time-varying angles of attack," *Chinese Journal of Aeronautics*, Vol. 32, No. 4, 2019, pp. 861–874. doi:10.1016/j.cja.2019.01.003.

[78] Amar Toor, engadget, "DARPA's Falcon HTV-2 hypersonic aircraft launches today, does New York to LA in 12 minutes (update: lost in flight)," https://www.engadget.com/2011-08-11-darpas-falcon-htv-2-hypersonic-aircraft-launches-today-does-ne.html, 2011. Accessed March 22, 2024.

[79] Scott, M., "Development and Modelling of Expansion Tubes," Ph.D. thesis, the University of Queensland, St. Lucia, Australia, 2006.

[80] James, C., Gildfind, D., Lewis, S., Morgan, R., and Zander, F., "Implementation of a state-to-state analytical framework for the calculation of expansion tube flow properties," *Shock Waves*, Vol. 28, No. 2, 2018, pp. 349–377. doi:10.1007/s00193-017-0763-3.

[81] James, C., "An Introduction to PITOT3," https://gdtk.uqcloud.net/pdfs/cmj-cfh-talk-07-2021.pdf, 2021. Accessed March 1, 2024.

[82] James, C. M., Lewis, S. W., Morgan, R. G., Liu, Y., and Lefevre, A., "Generating High-Speed Earth Reentry Test Conditions in an Expansion Tube," *Journal of Spacecraft and Rockets*, Vol. 58, No. 2, 2021, pp. 345–362. doi:10.2514/1.A34821.

[83] Chan, W. Y. K., Whitside, R. W., Smart, M. K., Gildfind, D. E., Jacobs, P. A., and Sopek, T., "Nitrogen driver for low-enthalpy testing in free-piston-driven shock tunnels," *Shock Waves*, Vol. 31, No. 6, 2021, pp. 541–550. doi:10.1007/s00193-021-01002-0.

[84] Stennett, S., Gildfind, D., Andrianatos, A., Morgan, R., Jacobs, P., James, C., Toniato, P., Chan, W., and Silvester, T., "Large-scale free-piston-driven multi-mode shock expansion tunnel," *Experiments in Fluids*, Vol. 65, No. 2, 2024. doi:10.1007/s00348-023-03756-y.

[85] Cullen, T., James, C., Gollan, R., and Morgan, R., "Development of a Total Enthalpy and Reynolds Number Matched Apollo Re-entry Condition in the X2 Expansion Tunnel," *31st International Symposium on Shock Waves*, Nagoya, Japan, July 9-14, 2017.

[86] Stennett, S., Gildfind, D., Andrianatos, A., Morgan, R., Jacobs, P., James, C., Toniato, P., Chan, W., and Silvester, T., "Large-scale free-piston-driven multi-mode shock expansion tunnel," *Experiments in Fluids*, Vol. 65, No. 2, 2024. doi:10.1007/s00348-023-03756-y.

[87] Chue, R., Tsai, C.-Y., Bakos, R., and Erdos, J., "NASA's HYPULSE Facility at GASL- A Dual Mode, Dual Driver Reflected-Shock/Expansion Tunnel," *Progress in Astronautics and Aeronautics*, edited by F. Lu and D. Marren, AIAA, 2002, Chap. 10, pp. 279–314. doi:https://doi.org/10.2514/5.9781600866678.0279.0314.

[88] Dufrene, A., MacLean, M., Parker, R., Wadhams, T., and Holden, M., "Characterization of the New LENS Expansion Tunnel Facility," *48th AIAA Aerospace Sciences Meeting Including the New Horizons Forum and Aerospace Exposition*, Orlando, FL, U.S.A., January 4-7, 2010.

[89] Stalker, R., "Hypervelocity Aerodynamics With Chemical Equilibrium," *Annual Review of Fluid Mechanics*, Vol. 21, 1989, pp. 37–60.

[90] INGER, G. R., "Similitude of Hypersonic Flows Over Slender Bodies in Nonequilibrium Dissociated Gases," *AIAA Journal*, Vol. 1, No. 1, 1963, pp. 46–53. doi:10.2514/3.1467.

[91] Hornung, H., *Experimental Hypervelocity Flow Simulations, Needs, Achievements and Limitations*, Tainan, Taiwan, Republic of China, December 6-9, 1993, pp. 1–10.

[92] Davies, W. R., and Bernstein, L., "Heat transfer and transition to turbulence in the shock-induced boundary layer on a semi-infinite flat plate," *Journal of Fluid Mechanics*, Vol. 36, No. 1, 1969, pp. 87–112. doi:10.1017/s0022112069001534.

[93] Lee, J. Y., and Lewis, M. J., "Numerical study of the flow establishment time in hypersonic shock tunnels," *Journal of Spacecraft and Rockets*, Vol. 30, No. 2, 1993, pp. 152–163. doi:10.2514/3.11523.

[94] Zhang, D., Deng, W., Xing, J., and Zhou, Z., "Numerical study of flow establishment process of engine in a shock tunnel," *Acta Astronautica*, Vol. 205, 2023, pp. 199–212. doi:10.1016/j.actaastro.2023.01.041.

[95] HOLDEN, M. S., "Establishment time of laminar separated flows," *AIAA Journal*, Vol. 9, No. 11, 1971, pp. 2296–2298. doi:10.2514/3.6512.

[96] Park, G., Hruschka, R., Gai, S. L., and Neely, A. J., "Flow establishment behind blunt bodies at hypersonic speeds in a shock tunnel," *28th International Congress on High-Speed Imaging and Photonics*, edited by H. Kleine and M. P. Butron Guillen, SPIE, 2008. doi:10.1117/12.822751.

[97] Park, G., Gai, S. L., and Neely, A. J., "Aerothermodynamics behind a blunt body at superorbital speeds," *AIAA journal*, Vol. 48, No. 8, 2010, pp. 1804–1816.

[98] James, C., Cullen, T., Wei, H., Lewis, S., Gu, S., Morgan, R., and McInytre, T., "Improved test time evaluation in an expansion tube," *Experiments in Fluids*, Vol. 59, No. 5, 2018, pp. 59–87. doi:\href{https://doi.org/10.1007/s00348-018-2540-1}{10.1007/s00348-018-2540-1}.

[99] Miller, C., and Moore, J., "Flow-establishment times for blunt bodies in an expansion tube," *AIAA Journal*, Vol. 13, No. 12, 1975, pp. 1676–1678. doi:\href{http://dx.doi.org/10.2514/3.7048}{10.2514/3.7048}.

[100] Mudford, N., and Stalker, R., "The production of pulsed nozzle flows in a shock tube," *9th Fluid and PlasmaDynamics Conference*, San Diego, C.A., U.S.A., 1976.

[101] Mudford, N., Stalker, R., and Shields, I., "Hypersonic nozzles for high enthalpy non equilibrium flow," *The Aeronautical Quarterly*, Vol. 31, No. 2, 1980, pp. 113–131.

[102] Stalker, R., and Mudford, N., "Unsteady shock propagation in a steady flow nozzle expansion," *Journal of Fluid Mechanics*, Vol. 241, 1992, pp. 525–548.

[103] Sakamoto, H., Sato, S., and Ohnishi, N., "Numerical Analysis of Shock Speed Attenuation in Expansion Tube," *AIAA Scitech 2021 Forum*, VIRTUAL EVENT, January 11-15 & 19-21, 2021. doi:10.2514/6.2021-0058.

[104] Furukawa, T., Aochi, T., and Sasoh, A., "Expansion Tube Operation with Thin Secondary Diaphragm," *AIAA Journal*, Vol. 45, No. 1, 2007, pp. 214–217. doi:10.2514/1.23846.

[105] Gildfind, D., "Development of High Total Pressure Scramjet Flows Conditions Using the X2 Expansion Tube," Ph.D. thesis, the University of Queensland, St Lucia, Australia, 2012.

[106] Trimpi, R., *A Preliminary Theoretical Study of the Expansion Tube, a New Device for Producing High-Enthalpy Short-Duration Hypersonic Gas Flows, NASA TR R-133*, NASA Langley Research Center, Langley Station, Hampton, VA, U.S.A., 1962.

[107] Paull, A., and Stalker, R. J., "Test flow disturbances in an expansion tube," *Journal of Fluid Mechanics*, Vol. 245, No. 1, 1992, pp. 493–521. doi:10.1017/S0022112092000569.

[108] Gildfind, D., Morgan, R., McGilvray, M., Jacobs, P., Stalker, R., and Eichmann, T., "Free-piston driver optimisation for simulation of high Mach number scramjet flow conditions," *Shock Waves*, Vol. 21, No. 6, 2011, pp. 559–572. doi:\href{http://dx.doi.org/10.2514/6.2012-5954}{10.2514/6.2012-5954}.

[109] Oswatitsch, K., *Similarity Laws for Hypersonic Flow*, Vieweg+Teubner Verlag, Wiesbaden, 1980, pp. 76–88. doi:10.1007/978-3-322-91082-0_8.

[110] Tsien, H., "Similarity Laws of Hypersonic Flows," *Journal of Mathematics and Physics*, Vol. 25, No. 1–4, 1946, pp. 247–251. doi:10.1002/sapm1946251247.

[111] Curtis, K., James, C., Lock, S., Lu, N., and Lewis, S., "Optimisation of super orbital Earth re-entry conditions in an expansion tube," *AIAA AVIATION 2022 Forum*, Chicago, IL, U.S.A. & Virtual, June 27-July1, 2022.

[112] Davey, M., "A Hypersonic Nozzle for the X3 Expansion Tube," Bachelor of engineering thesis, the University of Queensland, St. Lucia, Australia, 2006.

[113] Steer, J., Collen, P. L., Glenn, A. B., Sopek, T., Hambidge, C., Doherty, L. J., McGilvray, M., Loehle, S., and Walpot, L., "Experimental Study of a Galileo Sub-Scale Model at Ice Giant Entry Conditions in the T6 Free-Piston Driven Wind Tunnel," *AIAA SCITECH 2023 Forum*, American Institute of Aeronautics and Astronautics, 2023. doi:10.2514/6.2023-1339.

[114] Toniato, P., Gildfind, D. E., Jacobs, P. A., and Morgan, R. G., "Expansion tube nozzle design using a parallel simplex algorithm," *Shock Waves*, Vol. 30, No. 2, 2019, pp. 185–199. doi: 10.1007/s00193-019-00930-2.

[115] Toniato, P., "Free-jet testing of a Mach 12 scramjet in an expansion tube," Ph.D. thesis, the University of Queensland, St Lucia, Australia, 2019.

[116] MacLean, M., Marineau, E., Parker, R., Dufrene, A., Holden, M., and DesJardin, P., "Effect of Surface Catalysis on Measured Heat Transfer in Expansion Tunnel Facility," *Journal of Spacecraft and Rockets*, Vol. 50, No. 2, 2013, pp. 470–475.